な結果が得られた[10]。加えて，前述のようにサバイビンは大部分の癌で高発現しているため，Surv.m-CRAはほぼ全ての種類の癌を治療対象とできるという長所を持つ。

現在我々は，この独自のm-CRA技術によりSurv.m-CRAをさらに精巧に改良していると同時に，第二，第三弾の新規m-CRAも開発しているところである。最終的には，完全に癌細胞だけを認識するm-CRAを開発し，それを癌の主結節に注射すれば主結節を細胞死に陥らせ，さらにそのm-CRAは体内を駆け巡って全身の転移巣を探し出して副作用なく根絶するという，究極の治療法を確立することを目指している。また一方，m-CRAの作製技術，Surv.m-CRAとも，特許出願により知財確保もしており，最終的には本邦での国民福祉の向上を目指し，早期の臨床試験，そして一般医薬化を最終目標とした産業界への技術移転，起業化なども併せて目指して行きたいと思っている。

Ⅲ．再生医学

(1) 生体内再生医学（*in vivo* 再生療法）

再生医学（医療）は，「主に生物学的な知見の応用と技術により，障害・疾病で失われた組織を補完する治療法の研究」を総称とする新たな医学，医療であり，その開発には社会的にも大きな期待が寄せられている。再生医学といっても，個々の内容，対象疾患によって様々ではあるが，大きく二つに分類できる[11]。第一の再生医学は，ある物質や遺伝子を体内に投与することにより，元来持っている生体の再生能力を劇的に賦活化し，病気を治療するというものであり，我々はこれを「生体内再生医学（*in vivo*再生療法）」と呼んでいる[12]。我々が先駆けとして報告したHGF（肝細胞増殖因子）[13,14]，そして最近報告したHB-EGF（ヘパリン結合EGF様増殖因子）[15]による劇症肝炎の治療は，理想的な生体内再生治療法の代表であるので，これらを紹介する（図４）。

劇症肝炎とは急性肝炎患者の１～２％にみられるもので，急激に進展する広範性肝細胞死がその病態であるが，未だ効果的な治療法がないために，数日から数週間で40～70％の患者は死亡するという難治性疾患である。我々はまずFasとエンドトキシンの２種類のマウスモデルにて，肝栄養因子のHGFの投与により，肝細胞死を強力に抑制し生存率を劇的に向上させうることを見いだした[13,14]。さらに我々は最近，別の肝栄養因子であるHB-EGFが，HGFより強力に肝障害抑制と肝再生誘導作用を示すことを見出し，より効果的な劇症肝炎治療法となるHB-EGF生体内肝再生療法を開発した[15]。このように，再生誘導因子を治療薬として投与することで，生体内で病気の進展が止まり同時に障害臓器が再生治癒していくという「生体内再生医学（*in vivo*再生医療）」は，臨床的にも応用し易く，まさに理想的な治療法といえる（図４）。但しこれは生後もある程度の再生能力を保持している臓器，すなわち血球，皮膚，肝臓，などの臓器では最大の効果を示すが，生後は再生能力が失われている心臓，中枢神経などの臓器は，増殖因子のみでは生体内で再生が効率的に誘導されることはないため，これらの臓器疾患には第二の再生医学の開発が必要となる。

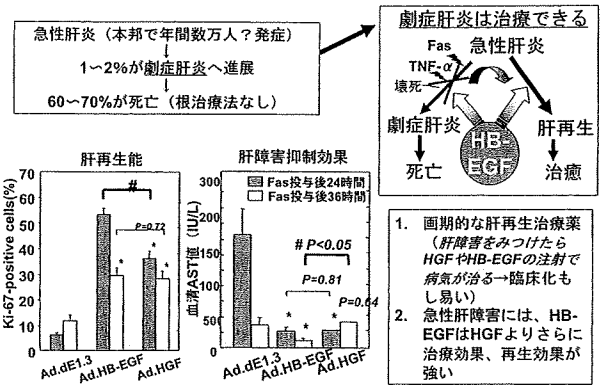

図４．劇症肝炎への生体内再生医学

(2) ES細胞による再生医学（再建療法）

第二の再生医学は，体外で何らかの細胞から目的の細胞や組織を分化誘導して創造し，それを障害臓器に細胞（組織）移植して治療するというもので，つまり臓器移植に代わる「再建療法」である。その源の細胞として，我々はES（胚性幹）細胞を選び，心筋と神経の研究を行っている[11]。循環器疾患は先進諸国の三大死因の一つであるが，種々の心疾患後の終末病態の心不全に対する根治療法は，現在のところは心臓移植しかない。しかし心臓移植は，その患者数（本邦だけでも循環器疾患で毎年15万人が死亡）に比べて圧倒的にドナーは不足しており，また加えて多額な経費，手術侵襲など，とても万人への一般医療と成り得るものではない。一方，近年の動物レベルの研究によると，臓器ではなくとも心筋の「細胞」の移植でも，心筋梗塞などではその病巣に生着し機能することが示唆されている。即ち，いかなる細胞種にでも分化できる多能性を保持したまま無尽蔵に増やす事ができるES細胞から，体外で目的の心筋細胞を創造することができ，その目的の心筋細胞種だけを単離することができれば，ES細胞由来の心筋細胞移植療法が確立できる可能性がでてくる。

そのためには第一に，心筋細胞を優位に誘導する方法の確立が必要である。我々はまず，胚様体形成法（初期胚の三葉形成を体外で模倣する方法）にFibroblast growth factor-2，Bone morphogenetic protein-2を至適濃度で至適のタイミングで加える事で，マウスES細胞から

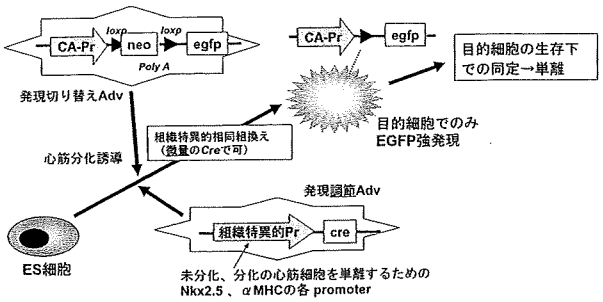

図5．Adenoviral conditional targeting in ES cell法

心筋細胞を効率よく分化誘導できることを見いだした[16]。次にヒトES細胞でも同様に心筋細胞の分化誘導の研究を行ったが，マウスES細胞に比べヒトES細胞は操作に技術的制約があり，胚様体形成の効率も悪かった。そこで間葉系細胞と共培養することで心筋の分化誘導ができないか，様々な細胞をスクリーニングし，ある細胞と共培養するとマウス，ヒトES細胞でも心筋細胞が誘導できることを見いだした[11]。但しヒトES細胞における心筋分化誘導効率はマウスES細胞ほど高くなく，あるいは安定性などで改善すべき問題があり，さらなる方法の改良を試みている。

さて一方，ES細胞より目的の心筋細胞を分化誘導できるとなれば，次にその目的細胞のみを純粋に単離，同定する技術が必要となる。細胞膜表面抗原マーカーを有する血球・血管系などのような一部の細胞種は，蛍光抗体法で目的細胞を可視化後，セルソーターで分離する技術が確立されている。しかしマーカーとなる細胞表面抗原がない，心筋細胞や神経細胞のような多くの細胞種には，組織特異的に発現する遺伝子のプロモーター制御下にレポーター遺伝子を安定発現するES細胞株を作製するという方法が，これまで唯一の戦略であった。我々は特にこれまでに報告のない，できるだけ初期の心筋系統細胞を同定，単離しようと試み，心臓の発生初期に発現する転写因子のNkx2.5遺伝子のプロモーターでGFPを安定発現するES細胞株を多数作製し検証したが，ES細胞から効率よく心筋分化誘導はできているのにも関わらず，GFPで可視化される細胞は全く認められなかった。このように従来の方法は材料作製に多大な労力と時間を費やす上に成功の保証がない不確実な方法で，特に分化初期の細胞には有効ではないことが明確となり，つまりこの問題の根本解決こそが，ES細胞再生医学一般における最重要課題であると分かった。

我々はプロモーターアッセイで，転写因子Nkx2.5，そしてサルコメア蛋白αMHCのプロモーター活性も，一般の発現実験に用いるCAGプロモーター活性より桁違いに低いことを明らかにし，つまり組織特異的プロモーターは活性強度が低すぎるということが従来法の根本原因であることが分かった。そこで我々は，アデノウイルスベクターとリコンビネーションシステムのAdenoviral conditional targeting法をES細胞の分化系に用い，簡単効率よく遺伝子導入・発現し，リコンビネーション反応でプロモーターの組織特異性を保持したままその活性を上昇させることでこの問題を解決し，ES細胞由来の目的細胞を簡単，確実に同定・単離することに成功した（図5）[17]。実際，Nkx2.5，αMHCの各プロモーターを含む調節アデノウイルスを用いた本法で，目的細胞が生存下で蛍光可視化され，マウスES細胞の心筋分化誘導が進むにつれ，この可視化細胞も増加していった。さらにセルソーターで各々の目的細胞を単離したところ，αMHC調節アデノウイルスで単離した細胞は，単一細胞化して培養しても自動収縮をくり返し，サルコメア構成蛋白質を発現することから，成熟心筋の性質を持つ細胞種と考えられた。一方，Nkx2.5調節アデノウイルスによって単離された細胞は，収縮能もサルコメア構造も認めず，さらにDNAマイクロアレイによる網羅的な遺伝子発現解析では未分化と心筋系統の両マーカーを混在して発現していた。よってこの細胞は，未だES細胞から単離されていない，心筋系統の拍動前の未分化初期細胞であろうという，非常に興味深い所見であった。また我々は，DNAマイクロアレイ解析で，この細胞から幾つかの重要と思われる未知遺伝子を同定しており，現在その幾つかの遺伝子の機能解析を行なっているところである。このように本法を用いれば，理論的には，いかなる組織・細胞系でも，興味ある遺伝子発現様態にのみ依存して，プロモーター活性に依存することなく，いかなる目的細胞でも確実に可視化することができると思われる。単離できた細胞は再生医療の移植用のドナー細胞として利用できるのはいうまでもなく，上記で示したように発生学の画期的な新しい実験手法としても，非常に有用と思われる。今後は，ヒトES細胞とこのオリジナル技術を基盤として，心疾患モデル動物での治療実験による細胞移植療法の開発，心筋の初期発生における新規分子の同定とメカニズムの解明など，研究を進めていきたいと思っている。

Ⅳ．高次脳機能のエピジェネティック分子制御の解明

最後に，最近始めた我々の脳研究を紹介する。Rett症候群は一万人に一人の発症と女性の精神発達遅滞で最も頻度が高い疾患で，一歳頃より精神遅滞・自閉的傾向，てんかん，発達停滞などを特徴とする神経疾患であり，効果的治療法は未だない。Rett症候群の原因は長年不明であったが，DNAのメチル化部位に直接結合して標的遺

伝子をエピジェネティックに発現抑制しているMeCP2遺伝子の変異が原因遺伝子と最近分かり，さらにRett症候群のモデルマウスであるMeCP2遺伝子欠損マウスも最近作製されたばかりである。しかしRett症候群の病態，病因とも未だ不明の部分が多く，MeCP2の生理的役割とメカニズムについても，Brain-derived neurotrophic factor（BDNF）のプロモーター部にMeCP2が直接結合して発現制御しているという報告以外，未知の部分が多く，MeCP2からの高次脳機能のメカニズム解明というのは世界的にも注目を浴びている。

我々はいち早くRett症候群モデルマウスのMeCP2欠損マウスを入手し，MeCP2発現アデノウイルスを作製し，遺伝子治療実験を行ってきた。またこれまでのES細胞の技術と経験を生かし，同様にES細胞の神経分化系で細胞，遺伝子レベルでそのメカニズムの解明の研究を進めている。我々は本研究には約3年前より取り組んだばかりで未だ進行中の段階ではあるが，高次脳機能のエピジェネティック分子制御の機構は全く未知なだけに，我々のオリジナルの研究手法により興味深い発見が得られるのではないかと思いながら研究を進めている。

V. 結　語

以上のように，我々の行っている，遺伝子治療，再生医学，脳の三分野における主な研究について述べた。これらの研究成果は特許出願して知財を確保しており，産学協同による技術移転，あるいは自身での起業化などにより，新しい治療法の本邦での一般医療化の実現を目指していきたいと思っている。鹿児島大学は歴史ある国立大学（法人）であり，また鹿児島の風土は歴史的にも証明されているように，独自の世界を築くための力を付与してくれるものと思っている。真のオリジナルの治療法を鹿児島から世界に発信し，最終的に本邦の国民福祉の向上に少しでも貢献できるよう，今後は鹿児島大学の基礎，臨床，そして他学部の諸先生と共同研究を積極的に進めて行きたいと思っている。

最後に私事で恐縮だが，私の実家は開業医で親族の多くも医師という環境で育ったため，医学部生の頃は，自分の進路として，患者と直接接する臨床医以外は想像したこともなかった。しかし実際に小児科研修医として臨床の現場に出てみて，根治療法のない病気は未だ多く，そして多くの患者さんが亡くなっておられることを現実として知った。臨床に近い基礎医学ということで大学院は病理学を選んだが，研究に関わるにつれ，分子生物学のより専門的な知識と遺伝子工学の強力な新技術を身につけ，自分自身で直接に新しい治療法を開発できるような研究に携わってみたいと思い憧れるようになり，遺伝子組換えの真似事を始めた。それからは国内外の様々な専門施設に所属し，13年前より遺伝子治療，10年前より再生医学，3年前からは脳と，独自に研究領域を広げてきた。ともかく15年前の「自身の手で治療法を開発できるようになりたい」という憧れが，今も私の先端医学開発に関わる研究のモチベーションの源となっている。私個人の能力，小研究室の規模を遥かに超える研究内容に小さな研究室で取り組んでしまっていることに加え，私はオリジナリティーを最重視するため（科学的理由だけでなく，上記のように将来社会還元するためには知財確保が必要なため），基盤の研究材料と技術開発から自身の研究室で行うため，時間が非常にかかることもあり，まだまだ発展途上の研究が多い。15年前に憧れていた先端治療法開発の研究に現在自身が毎日取り組めることに感謝するとともに，初めて患者を受け持った時の感動，自分自身で大腸菌での遺伝子組換え実験を最初に行った時の感動をいつまでも忘れる事無く，今後も研究と教育に邁進したいと思っている。

文　献

1. Chen SH, Chen XH, Wang Y, Kosai K, Finegold MJ, Rich SS, et al. Combination gene therapy for liver metastasis of colon carcinoma in vivo. Proc Natl Acad Sci U S A 1995; 92: 2577-2581.
2. Chen SH, Kosai K, Xu B, Pham-Nguyen K, Contant C, Finegold MJ, et al. Combination suicide and cytokine gene therapy for hepatic metastases of colon carcinoma: sustained antitumor immunity prolongs animal survival. Cancer Res 1996; 56: 3758-3762.
3. Terazaki Y, Yano S, Yuge K, Nagano S, Fukunaga M, Guo ZS, et al. An optimal therapeutic expression level is crucial for suicide gene therapy for hepatic metastatic cancer in mice. Hepatology 2003; 37: 155-163.
4. Nagano S, Yuge K, Fukunaga M, Terazaki Y, Fujiwara H, Komiya S, et al. Gene therapy eradicating distant disseminated micro-metastases by optimal cytokine expression in the primary lesion only: novel concepts for successful cytokine gene therapy. Int J Oncol 2004; 24: 549-558.
5. Fukunaga M, Takamori S, Hayashi A, Shirouzu K, Kosai K. Adenoviral herpes simplex virus thymidine kinase gene therapy in an orthotopic lung cancer model. Ann Thorac Surg 2002; 73: 1740-1746.
6. Ikoma T, Takahashi T, Nagano S, Li YM, Ohno Y,

Ando K, et al. A definitive role of RhoC in metastasis of orthotopic lung cancer in mice. Clin Cancer Res 2004; 10: 1192-1200.
7．室伏善照，神圃純一，小戝健一郎，新世代癌遺伝子治療のための多因子で増殖制御/癌特異化するアデノウイルスの作製法．細胞工学 2005; 25: 60-66.
8．神圃純一，室伏善照，小戝健一郎，多因子で増殖制御/癌特異標的化するアデノウイルスベクターのはじめての標準化作製技術．バイオテクノロジージャーナル 2005; 5: 728-731.
9．Nagano S, Oshika H, Fujiwara H, Komiya S, Kosai K. An efficient construction of conditionally replicating adenoviruses that target tumor cells with multiple factors. Gene Ther 2005; 12: 1385-1393
10. Kamizono J, Nagano S, Murofushi Y, Komiya S, Fujiwara H, Matsuishi T, et al. Survivin-responsive conditionally replicating adenovirus exhibits cancer-specific and efficient viral replication. Cancer Res 2005; 65: 5284-5291.
11. 高橋知之，藤原久義，國貞隆弘，小戝健一郎．【ヒトおよびサルのES細胞】ES細胞再生医学の新技術開発 ヒトES細胞と遺伝子治療技術．再生医療 2006; 5: 43-51.
12. 高橋知之，小戝健一郎．HGF 急性／劇症肝炎．松本邦夫，田畑安彦 編．細胞増殖因子と再生医療．大阪：メディカルレビュー社，2006: 199-204.
13. Kosai K, Matsumoto K, Nagata S, Tsujimoto Y, Nakamura T. Abrogation of Fas-induced fulminant hepatic failure in mice by hepatocyte growth factor. Biochem Biophys Res Commun 1998; 244: 683-690.
14. Kosai K, Matsumoto K, Funakoshi H, Nakamura T. Hepatocyte growth factor prevents endotoxin-induced lethal hepatic failure in mice. Hepatology 1999; 30: 151-159.
15. Khai NC, Takahashi T, Ushikoshi H, Nagano S, Yuge K, Esaki M, et al. In vivo hepatic HB-EGF gene transduction inhibits Fas-induced liver injury and induces liver regeneration in mice: a comparative study to HGF. J Hepatol 2006; 44: 1046-1054.
16. Kawai T, Takahashi T, Esaki M, Ushikoshi H, Nagano S, Fujiwara H, et al. Efficient cardiomyogenic differentiation of embryonic stem cell by fibroblast growth factor 2 and bone morphogenetic protein 2. Circ J 2004; 68: 691-702.
17. Takahashi T, Kawai T, Ushikoshi H, Nagano S, Oshika H, Inoue M, et al. Identification and isolation of embryonic stem cell-derived target cells by adenoviral conditional targeting. Mol Ther 2006; 14: 673-683.

Reprinted from

Journal of Neurosurgery: Pediatrics

Occult spinal canal stenosis due to C-1 hypoplasia in children with Down syndrome

SHUNJI MATSUNAGA, M.D., PH.D., TAKANORI IMAKIRE, M.D., HIROAKI KOGA, M.D., PH.D., YASUIRO ISHIDOU, M.D., PH.D., HIROMI SASAKI, M.D., EIJI TAKETOMI, M.D., PH.D., MASARU HIGO, M.D., PH.D., HIROSHI TANAKA, M.D., PH.D., AND SETSURO KOMIYA, M.D., PH.D.

DECEMBER 2007 Volume 107, Number 6:457-459

American Association of Neurological Surgeons

WWW.THEJNS.ORG

The American Society of Pediatric Neurosurgeons

J Neurosurg (6 Suppl Pediatrics) 107:457–459, 2007

Occult spinal canal stenosis due to C-1 hypoplasia in children with Down syndrome

SHUNJI MATSUNAGA, M.D., PH.D.,[1] TAKANORI IMAKIIRE, M.D.,[1] HIROAKI KOGA, M.D., PH.D.,[1] YASUHIRO ISHIDOU, M.D., PH.D.,[2] HIROMI SASAKI, M.D.,[2] EIJI TAKETOMI, M.D., PH.D.,[3] MASARU HIGO, M.D., PH.D.,[4] HIROSHI TANAKA, M.D., PH.D.,[5] AND SETSURO KOMIYA, M.D., PH.D.[2]

[1]Department of Orthopaedic Surgery, Imakiire General Hospital; [2]Department of Orthopaedic Surgery, Graduate School of Medical and Dental Sciences, Kagoshima University; [3]Department of Orthopaedic Surgery, Kagoshima Red-Cross Hospital; [4]Department of Orthopaedic Surgery, Kagoshima Prefectural Crippled Children's Hospital; and [5]Department of Pediatrics, Kibougaoka Hospital, Kagoshima, Japan

Object. Little has been published about subclinical spinal canal stenosis due to C-1 hypoplasia in patients with Down syndrome. In this paper the authors performed a matched comparison study with cross-sectional survey to investigate occult spinal canal stenosis due to C-1 hypoplasia in children with Down syndrome.

Methods. A total of 102 children with Down syndrome ranging in age from 10 to 15 years were matched according to age and physique with 176 normal children. In all participants, the anteroposterior (AP) diameter of C-1 and the atlas–dens interval (ADI) were measured on plain lateral x-ray images of the cervical spine. The cross-sectional area of the atlas was also measured from a cross-sectional computed tomography image of C-1.

Results. Eight children (6.7%) with Down syndrome developed atlantoaxial subluxation associated with myelopathy. The difference in the ADI between the patients and controls was not statistically significant. The average AP diameter of the atlas and the spinal canal area along the cross-section of the atlas were significantly smaller in children with Down syndrome than those in the control group.

Conclusions. Atlantoaxial instability and occult spinal canal stenosis due to C-1 hypoplasia in patients with Down syndrome may significantly increase the risk of myelopathy. *(DOI: 10.3171/PED-07/12/457)*

KEY WORDS • atlantoaxial subluxation • atlas–dens interval • Down syndrome • hypoplasia of atlas • myelopathy • pediatric neurosurgery

It is well known that in children with Down syndrome, atlantoaxial subluxation associated with os odontoideum may cause neurological symptoms.[3,5,8,10] However, C-1 hypoplasia has not been recognized as a risk factor for occurrence of myelopathy. Subclinical spinal canal stenosis due to a hypoplastic posterior arch of the atlas has been reported in patients with Klippel–Feil syndrome.[1,12] However, little has been published on the occurrence of myelopathy related to atlantoaxial subluxation in children with Down syndrome, especially in conjunction with subclinical spinal canal stenosis due to hypoplasia of the atlas. We performed a matched comparison study with cross-sectional survey to confirm the existence of spinal canal stenosis due to hypoplastic posterior arch of the atlas in children with Down syndrome.

Abbreviations used in this paper: ADI = atlas–dens interval; AP = anteroposterior; CT = computed tomography.

Clinical Material and Methods

This study was designed as a matched comparison study with a cross-sectional survey. There were 102 children (70 boys and 32 girls) with Down syndrome who ranged in age from 10 to 15 years. These patients were age matched with 176 asymptomatic children (110 boys and 66 girls). The height and weight of children in the two groups were matched (Table 1). The asymptomatic children were children of the authors and their friends. The diagnosis of Down syndrome was made based on the characteristic clinical futures and chromosome abnormality (trisomy 21). The necks of the children were positioned carefully so that accurate lateral radiographs could be obtained. Radiographs were obtained with a constant tube-to-film and spine-to-film distance of 150 cm. In all candidates, the AP diameter of the atlas and ADI were measured from plain lateral flexion and extension dynamic x-ray images of the cervical spine. The cross-sectional area of the atlas (Fig. 1) was also measured

TABLE 1

*Height and weight of patients with Down syndrome and control individuals by age**

Age (yrs), Sex	Height (cm)		Weight (kg)	
	Patients w/ Down Syndrome	Control Individuals	Patients w/ Down Syndrome	Control Individuals
10, M	134.8 ± 2.7	135.3 ± 2.9	34.6 ± 2.7	34.3 ± 2.2
10, F	135.9 ± 4.5	136.3 ± 3.1	33.7 ± 4.4	33.3 ± 3.9
11, M	141.7 ± 4.2	141.8 ± 2.7	38.7 ± 4.8	38.8 ± 2.8
11, F	141.8 ± 3.4	142.3 ± 3.9	37.8 ± 3.5	37.2 ± 3.7
12, M	152.9 ± 4.4	153.1 ± 3.3	43.4 ± 4.4	43.1 ± 3.6
12, F	150.1 ± 3.9	150.7 ± 4.2	44.1 ± 3.1	43.7 ± 4.9
13, M	157.4 ± 4.2	157.9 ± 3.8	47.2 ± 3.2	46.9 ± 3.1
13, F	154.0 ± 3.2	154.2 ± 4.4	46.5 ± 3.8	46.2 ± 4.1
14, M	160.8 ± 4.1	161.2 ± 4.7	56.8 ± 3.1	56.3 ± 4.0
14, F	156.1 ± 3.3	156.4 ± 4.8	50.9 ± 3.9	50.2 ± 3.1
15, M	165.8 ± 4.1	166.2 ± 4.7	58.8 ± 3.7	58.2 ± 4.2
15, F	157.8 ± 4.1	157.9 ± 3.6	53.3 ± 3.1	52.9 ± 4.1

* Values are presented as the mean ± standard deviation. The probability values of age- and weight-matched patients were not significant.

from a cross-sectional CT image of the atlas. The cross-sectional area was divided into small grid cells and analyzed with a computer by using an integration method. All the measurements were completed at the first examination. We obtained the informed consent from the individuals and their parents prior to the examination and obtaining radiographs and CT scans. The parents were fully aware that the data from the cases and controls would be submitted for publication, and the approval was also obtained from our institutional review board.

Statistical Analysis

Parametric statistical analysis was performed using Student t-test with a 95% confidence interval.

Results

Eight children with Down syndrome (three boys and five girls, age range 10–13 years) were identified with atlantoaxial subluxation (Table 2); an incidence of 6.7% (4.3% in boys and 15.7% in girls). Two of the eight children had fixed atlantoaxial subluxation and the remaining six children had reducible atlantoaxial subluxation. The condition of four patients was complicated by os odontoideum. All patients with atlantoaxial subluxation exhibited spastic gait, hyperreflexia, pathological reflex, and disturbance of finger movement. We recommended surgery to the eight patients,

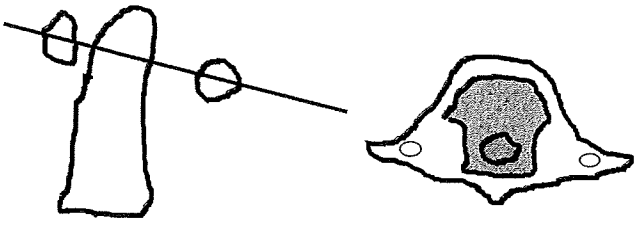

FIG. 1. Illustrations showing the method of measurement of the C-1 cross-sectional area on the CT scans. *Left:* The *line* indicates the slice level of the atlas that will be used for the CT scan. *Right:* The *shaded area* indicates the cross-sectional area of C-1.

TABLE 2

*Characteristics of patients who exhibit atlantoaxial subluxation**

Case No.	Age (yrs), Sex	ADI (mm)	Os Odontoideum	Hyperreflexia	Spastic Gait
1	10, M	6	−	+	+
2	10, F	8	+	+	+
3	11, M	7	+	+	+
4	10, F	6	−	+	+
5	11, F	7	+	+	+
6	12, F	8	+	+	+
7	12, F	8	−	+	+
8	13, M	9	−	+	+

* + = present, − = absent.

but we could not obtain agreement. The ADI ranged from 6 to 9 mm among the patients who exhibited atlantoaxial subluxation, and all patients exhibited hypoplasia of atlas. The mean (± standard deviation) ADI was 2.5 ± 1.0 mm in all children with Down syndrome and 2.2 ± 1.0 mm in healthy children. The difference between the two groups was not statistically significant in boys or girls. The average AP diameters of the atlas were significantly smaller in patients with Down syndrome than in controls. The results were the same in boys and girls (Table 3). The cross-sectional area of the atlas was significantly smaller in children with Down syndrome than in the control group (Table 4). Figure 2 provides an example of CT images of a patient with Down syndrome and a healthy male control of the same age. The AP diameter and cross-sectional area of the atlas were smaller in the patient with Down syndrome.

Discussion

Atlantoaxial dislocation in patients with Down syndrome was reported by Tishler and Martel[10] in 1965 and by Dzenitis[3] in 1966. Since then, many articles[2,4,5,7–9,11,12] have appeared in the literature detailing imaging-documented atlantoaxial instability in children with Down syndrome.

The present study suggests that occult spinal canal steno-

TABLE 3

Anteroposterior diameter of C-1 on plain lateral x-ray images

Sex	AP Diameter in mm (no. of children)		p Value*
	Patients w/ Down Syndrome	Control Individuals	
boy	16.1 ± 2.5 (70)	21.3 ± 2.1 (110)	<0.005
girl	15.3 ± 2.9 (32)	19.4 ± 2.3 (66)	<0.005
total	15.8 ± 2.7 (102)	20.3 ± 2.2 (176)	<0.005

* Values are statistically significant.

TABLE 4

Cross-sectional area of C-1 on CT scanning

Sex	Area in mm^2 (no. of children)		p Value*
	Patients w/ Down Syndrome	Control Individuals	
boy	523.7 ± 52.3 (70)	615.9 ± 51.1 (110)	<0.005
girl	498.3 ± 49.6 (32)	589.8 ± 51.9 (66)	<0.005
total	505.6 ± 51.9 (102)	602.7 ± 51.6 (176)	<0.005

* Values are statistically significant.

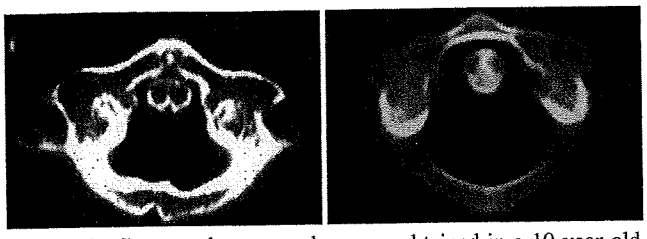

FIG. 2. Computed tomography scans obtained in a 10-year-old patient with Down syndrome *(left)* and a 10-year-old healthy individual *(right)*. The cross-sectional area of C-1 was 512 mm^2 in the patient and 690 mm^2 in the control.

sis exists in patients with Down syndrome. To our knowledge, this is the first matched-comparison study that has examined occult spinal canal stenosis due to hypoplasia of the C-1 posterior arch in patients with Down syndrome. In 1992, Martich et al.[6] reported hypoplastic posterior arch of atlas in children with Down syndrome; however, that study was not a matched comparison, and the children were younger (2–3 years old). In our study, the hypoplasia of C-1 in children with Down syndrome was statistically significant. The pathomechanism of myelopathy in patients with Down syndrome has not been clarified. However, the occult spinal canal stenosis due to C-1 hypoplasia must be a risk factor of myelopathy for patients with Down syndrome. All patients with atlantoaxial subluxation in the current study exhibited myelopathy. The ADI among the patients who exhibited myelopathy was less than 9 mm, which did not indicate severe atlantoaxial subluxation.

Conclusions

When dealing with children with Down syndrome, it must be remembered that the patients may have occult spinal canal stenosis which can cause myelopathy.

References

1. Chigira M, Kaneko K, Mashio K, Watanabe H: Congenital hypoplasia of the arch of the atlas with abnormal segmentation of the cervical spine. **Arch Orthop Trauma Surg 113:**110–112, 1994
2. Cullen S, O'Connell E, Blake NS, Ward OC: Atlantoaxial instability in Down's syndrome: clinical and radiological screening. **Ir Med J 82:**64–65, 1989
3. Dzenitis AJ: Spontaneous atlanto-axial dislocation in a mongoloid child with spinal cord compression. Case report. **J Neurosurg 25:**458–460, 1966
4. el-Khoury GY, Clark CR, Wroble RR: Fixed atlantoaxial rotary deformity with bilateral facet dislocation. **Skeletal Radiol 13:** 217–220, 1985
5. Martel A, Uyham R, Stimson CW: Subluxation of the atlas causing spinal cord compression in a case of Down's syndrome with a "manifestation of an occipital vertebra". **Radiology 93:** 129–132, 1969
6. Martich V, Ben-Ami T, Yousefzadeh DK, Roizen NJ: Hypoplastic posterior arch of C-1 in children with Down syndrome: a double jeopardy. **Radiology 183:**125–128, 1992
7. Pueschel SM, Findley TW, Furia J, Gallagher PL, Scola FH, Pezzullo JC: Atlantoaxial instability in children with Down's syndrome: roentgenographic, neurological, and somatosensory evoked potential studies. **J Pediatr 110:**515–521, 1987
8. Pueschel SM, Herndon JH, Gelch MM, Senft KE, Scola FH, Goldberg MJ: Symptomatic atlantoaxial subluxation in persons with Down syndrome. **J Pediatr Othop 4:**682–688, 1984
9. Semine AA, Ertel AN, Goldberg MJ, Bull MJ: Cervical spine instability in children with Down syndrome (trisomy 21). **J Bone Joint Surg Am 60:**649–652, 1978
10. Tishler JM, Martel W: Dislocation of the atlas in mongolism: preliminary report. **Radiology 84:**904–906, 1965
11. Tredwell SJ, Newman DE, Lockitch G: Instability of the upper cervical spine in Down syndrome. **J Pediatr Orthop 10:**602–606, 1990
12. Tubbs RS, Oakes WJ, Blount JP: Isolated atlantal stenosis in a patient with idiopathic growth hormone deficiency, and Klippel-Feil and Duane's syndromes. **Childs Nerv Syst 21:**421–424, 2005

Manuscript submitted May 8, 2007.
Accepted August 20, 2007.

Address correspondence to: Shunji Matsunaga, M.D., Ph.D., Department of Orthopaedic Surgery, Imakiire General Hospital, 4-16, Schimotatsuo, Kagoshima 892-8502, Japan. email: shunji@m.kufm.kagoshima-u.ac.jp.

MOLECULAR AND CELLULAR BIOLOGY, Aug. 2007, p. 5650–5663 Vol. 27, No. 16
0270-7306/07/$08.00+0 doi:10.1128/MCB.00130-07

Stage-Specific Secretion of HMGB1 in Cartilage Regulates Endochondral Ossification▽†

Noboru Taniguchi,[1] Kenji Yoshida,[1] Tatsuo Ito,[1] Masanao Tsuda,[1] Yasunori Mishima,[1] Takayuki Furumatsu,[1] Lorenza Ronfani,[2] Kazuhiro Abeyama,[4] Ko-ichi Kawahara,[4] Setsuro Komiya,[5] Ikuro Maruyama,[4] Martin Lotz,[1] Marco E. Bianchi,[2,3] and Hiroshi Asahara[1,6,7]*

Department of Molecular and Experimental Medicine, The Scripps Research Institute, 10550 North Torrey Pines Road, La Jolla, California 92037[1]; DIBIT, San Raffaele Scientific Institute, via Olgettina 58, 20132 Milano, Italy[2]; San Raffaele University, via Olgettina 58, 20132 Milano, Italy[3]; Department of Laboratory and Vascular Medicine, Graduate School of Medical and Dental Sciences, Kagoshima University, 8-35-1 Sakuragaoka, Kagoshima 890-8520, Japan[4]; Department of Orthopaedic Surgery, Graduate School of Medical and Dental Sciences, Kagoshima University, 8-35-1 Sakuragaoka, Kagoshima 890-8520, Japan[5]; National Center for Child Health and Development, 2-10-1 Okura, Setagaya, Tokyo 157-8535, Japan[6]; and SORST, Japan Science and Technology Agency, 4-1-8 Honcho, Kawaguchi, Saitama 332-0012, Japan[7]

Received 20 January 2007/Returned for modification 25 February 2007/Accepted 19 May 2007

High mobility group box 1 protein (HMGB1) is a chromatin protein that has a dual function as a nuclear factor and as an extracellular factor. Extracellular HMGB1 released by damaged cells acts as a chemoattractant, as well as a proinflammatory cytokine, suggesting that HMGB1 is tightly connected to the process of tissue organization. However, the role of HMGB1 in bone and cartilage that undergo remodeling during embryogenesis, tissue repair, and disease is largely unknown. We show here that the stage-specific secretion of HMGB1 in cartilage regulates endochondral ossification. We analyzed the skeletal development of *Hmgb1*$^{-/-}$ mice during embryogenesis and found that endochondral ossification is significantly impaired due to the delay of cartilage invasion by osteoclasts, osteoblasts, and blood vessels. Immunohistochemical analysis revealed that HMGB1 protein accumulated in the cytosol of hypertrophic chondrocytes at growth plates, and its extracellular release from the chondrocytes was verified by organ culture. Furthermore, we demonstrated that the chondrocyte-secreted HMGB1 functions as a chemoattractant for osteoclasts and osteoblasts, as well as for endothelial cells, further supporting the conclusion that *Hmgb1*$^{-/-}$ mice are defective in cell invasion. Collectively, these findings suggest that HMGB1 released from differentiating chondrocytes acts, at least in part, as a regulator of endochondral ossification during osteogenesis.

Bone formation occurs through two developmental processes: intramembranous ossification and endochondral ossification. Intramembranous ossification takes place in several craniofacial bones and the lateral part of clavicles, whereas endochondral ossification occurs in the long bones of the limbs, the basal part of the skull, vertebrae, ribs, and the medial part of the clavicles. In endochondral ossification, an intermediate step occurs during which cartilaginous templates prefigure future skeletal elements and play a major role in regulating the developing skeletal elements (33). First, mononucleated osteoclast precursors enter the mesenchyme surrounding the bone rudiments, proliferate, differentiate into tartrate-resistant acid phosphatase (TRAP)-positive cells, and migrate together with endothelial cells through the nascent bone collar (7). Subsequently, they invade the calcified cartilage, filling the core of the diaphysis while fusing and differentiating into mature osteoclasts, and transform the core of the bone into a marrow cavity (15). Osteoclasts are derived from hematopoietic precursor cells formed by the fusion of monocytic cells at the bone sites to be resorbed, whereas osteoblasts arise from multipotential mesenchymal cells and further differentiate into bone-lining cells and osteocytes (30).

These events, including osteoclast migration and angiogenesis during endochondral ossification, are tightly coordinated by extracellular factors, such as matrix metalloproteinases (MMPs) and vascular endothelial growth factor (VEGF) (37). When neovascularization of the cartilage anlage begins, membrane type 1 MMP (MT1-MMP) and MMP9 are expressed in the preosteoclasts and other chondroclastic cells of unknown origins (23). Mice deficient in *Mmp9* exhibit a delay in osteoclast recruitment in specialized invasion and bone resorption models in vitro (15). It is also reported that the deletion of functional *Mmp13* has profound effects on skeletal development (25). In *Mmp13*-null embryos, the growth plates were strikingly lengthened, a defect related predominantly to a delay in terminal events in the growth plates, with failure to resorb collagens, as well as a delay in ossification at the primary centers. In addition, VEGF signaling plays an important role of angiogenesis during skeletal development (59). Inhibition of VEGF by the administration of a soluble chimeric VEGF receptor protein to 24-day-old mice inhibited blood vessel invasion

* Corresponding author. Mailing address: Department of Molecular and Experimental Medicine, The Scripps Research Institute, 10550 North Torrey Pines Road, La Jolla, CA 92037. Phone: (858) 784-9026. Fax: (858) 784-2744. E-mail: asahara@scripps.edu.

† Supplemental material for this article may be found at http://mcb.asm.org/.

▽ Published ahead of print on 4 June 2007.

into the hypertrophic zone of long bone growth plates and resulted in impaired trabecular bone formation and expansion of the hypertrophic zone (17).

High mobility group box 1 protein (HMGB1) is a chromatin protein that is widely expressed and extremely conserved in mammals. There are three HMGB proteins: HMGB1, HMGB2, and HMGB3 with >80% amino acid identity, which are composed of two basic HMG-box domains (A and B) and a long acidic C-terminal tail (10). As a nuclear factor, HMGB1 acts as an architectural protein that can bend DNA to promote nucleoprotein interactions and facilitate diverse DNA modifications (2). Several groups have shown that HMGB1 also has an extracellular role as a proinflammatory cytokine (4, 51, 55). Two different routes for HMGB1 release into the extracellular milieu have been reported: active secretion by activated macrophages and monocytes (54) and passive release from necrotic or damaged cells (45). HMGB1 released by damaged cells acts as a chemoattractant for vascular smooth muscle cells and fibroblasts and induces cytoskeleton reorganization and cell migration (13). HMGB1 also promotes the migration of local stem cells, such as vessel-associated stem cells (mesoangioblasts) (38), and endothelial cells (32, 46), suggesting that HMGB1 is tightly connected to the process of tissue organization. The biological relevance of HMGB1 in vivo was shown in *Hmgb1*$^{-/-}$ mice, which have a highly pleiotropic phenotype such as the inability to use glycogen stored in the liver (11). These mice survive for several days if given glucose parenterally; however, mutants remained much smaller than control littermates and had arched backs, posterior limbs splayed wide apart, and abnormal gait. These findings suggested that HMGB1 may participate in not only tissue repair after injury but also the organization of bone and cartilage development.

We show here that the stage-specific secretion of HMGB1 in cartilage regulates endochondral ossification, in part, by acting as a chemotactic factor for the cells that invade at the primary ossification center. These findings highlight the potential role of HMGB1 in skeletal homeostasis.

MATERIALS AND METHODS

Mice. The *Hmgb1*$^{-/-}$ mutant mice used in the present study were described before (11), except for their background, which is now pure BALB/c. All animal experiments were performed according to approved protocols according to institutional guidelines at The Scripps Research Institute. Mouse embryos for histomorphometry were littermates from *Hmgb1*$^{+/-}$ parents. The genotype of the mice was determined by PCR analysis of tail DNA. The wild-type *Hmgb1* allele was detected by PCR with the primers wildtype-1 (5′-GCA GGC TTC GTT GTT TTC ATA CAG-3′) and wildtype-2 (5′-TCA AAG AGT AAT ACT GCC ACC TTC-3′), which generate a 495-bp fragment. The mutant *Hmgb1* allele was detected by using two primers complementary to the neomycin resistance gene—Neo-1 (5′-TGG TTT GCA GTG TTC TGC CTA GC-3′) and Neo-2 (5′-CCC AGT CAT AGC CGA ATA GCC-3′)—which generate a 336-bp fragment.

Histological analysis. Mice were sacrificed at various embryonic stages, dissected, and fixed in 4% paraformaldehyde–phosphate-buffered saline at 4°C overnight. Subsequently, they were processed, embedded in paraffin, and sectioned. For HMGB1 immunostaining, rabbit anti-HMGB1 antibody (Pharmingen, San Diego, CA) and chicken anti-HMGB1 antibody (Shino-Test, Kanagawa, Japan) were used for limb sections and organ culture sections, respectively (51). For CD31 immunostaining, embryos were infiltrated in 20% sucrose, followed by OCT embedding to stain with rat anti-PECAM antibody (Pharmingen) and von Kossa and Safranin O/Fast Green staining (47). Whole-mount alcian blue and alizarin red S staining of skeletons were done as described previously (31), and the longitudinal diameters of calvariae, as well as the lengths and alizarin-positive regions of tibias, were measured by micrometer. Detection of apoptotic cells in paraffin sections of limbs was based on a modification of genomic DNA utilizing terminal deoxynucleotidyl transferase (TUNEL [terminal deoxynucleotidyltransferase-mediated dUTP-biotin nick end labeling] assay) and indirect detection of positive cells by fluorescein conjugated anti-digoxigenin antibody using a MEBSTAIN Apoptosis Kit Direct (Medical and Biological laboratories, Nagoya, Japan). Immunofluorescence assay to determine HMGB1 translocation in chondrocytes was carried out with rabbit anti-HMGB1 antibody (Pharmingen) as described before (51).

Using a leukocyte acid phosphatase kit from Sigma (St. Louis, MO), TRAP staining was performed on paraffin sections according to the instructions provided by the manufacturer. The determination of the numbers and distribution of TRAP-positive cells in longitudinal sections of bones was done as described previously (7, 56).

In situ hybridization. Tissues were fixed in 4% paraformaldehyde–phosphate-buffered saline overnight at 4°C, processed, embedded in paraffin, and sectioned. RNA in situ hybridization was performed as described previously (3). Briefly, slides were deparaffinized, treated with proteinase K (1 μg/ml) for 20 min at 37°C, and hybridized with ^{35}S-labeled antisense riboprobes in hybridization buffer (50% deionized formamide, 300 mM NaCl, 20 mM Tris-HCl [pH 8.0], 5 mM EDTA, 0.5 mg of yeast tRNA/ml, 10% dextran sulfate, and 1× Denhardt solution) in a humidified chamber at 60°C overnight. After hybridization, the slides were treated with RNase A, washed to a final stringency of 50% formamide, 2× SSC (1× SSC is 0.15 M NaCl plus 0.015 M sodium citrate) at 60°C, dipped in emulsion, exposed for 3 days to 3 weeks, and developed. The probes for Indian hedgehog, MMP9, VEGF and MMP13, MT1-MMP, Runx2 and Osterix, and osteocalcin and osteopontin were provided by Y. Kawakami (Salk Institute), S. M. Krane (Harvard Medical School), Z. Werb (University of California, San Francisco), T. Vu (University of California, San Francisco), K. Nakashima (Tokyo Medical and Dental University), and S. Nomura (Osaka University Graduate School of Medicine), respectively. The HMGB1 probe was a 1.2-kb cDNA fragment encoding the COOH-terminal domain and the 3′-untranslated region (UTR). The Col1a1 probe was a 0.8-kb cDNA fragment encoding the COOH-terminal domain.

Organ culture. Metatarsal bones and tibiae were harvested from mouse embryos at embryonic day 15.5 (E15.5) and E14.5, respectively. They were cultured for 5 days in conditioned medium as described previously (20). The expression levels of HMGB1 and lactate dehydrogenase (LDH) in the supernatant were assessed by immunoblotting with rabbit anti-HMGB1 antibody (Pharmingen) and goat anti-LDH antibody (Chemicon, Temecula, CA) as described previously (45). Rib chondrocytes were purified from the ventral parts of rib cartilage of 2- to 4-day-old BALB/c mice (28), followed by induction of necrosis as described previously (45), and were used as a positive control for the HMGB1 protein. The concentrations of HMGB1 released into conditioned supernatant were measured in triplicate with an enzyme-linked immunosorbent assay (ELISA) using commercially available kits (Shino-Test) (57).

Preparation of osteoclasts and osteoblasts. Human osteoclast precursor cells (Poietics; Cambrex Bio Science Walkersville, Inc., Walkersville, MD) were cultured in alpha-minimal essential medium (alpha-MEM) containing 10% fetal bovine serum, penicillin-streptomycin, and HEPES containing alpha-MEM medium with receptor activator of nuclear factor B ligand (RANKL; PeproTech EC, Ltd., London, United Kingdom) and M-CSF (R&D Systems, Minneapolis, MN). Cells were incubated in a CO_2 incubator in a humidified atmosphere of 95% air and 5% CO_2 at 37°C. After complete osteoclast differentiation at day 7, the medium was replaced with serum-free alpha-MEM; the cells were starved for 2 h and then used for chemotaxis assays. MC3T3-E1 osteoblastic cells were purchased from the American Type Culture Collection (Manassas, VA) and cultured in alpha-MEM with 10% fetal bovine serum.

Chemotaxis assays. Chemotaxis assays were performed as described previously (22). The assays were carried out in Boyden chambers with polycarbonate filters with 9-μm pores (Corning Costar, Corning, NY). Osteoclasts were prepared by sequential treatment with trypsin, and the remaining cells were then gently lifted off the plates with a rubber policeman. The osteoclasts were seeded in 48-transwell plates in alpha-MEM containing 0.1% (wt/vol) Albumax and kept for 4 h with or without addition of rat cytokine-quality HMGB1 (obtained from HMGBiotech, Milan, Italy) and VEGF (R&D Systems). Invasion was determined as the ratio of osteoclasts that migrated through the collagen gel to reach the lower side of the membrane compared to the total number of osteoclasts in the insert. The chemotaxis assays for MC3T3-E1 cells were also performed

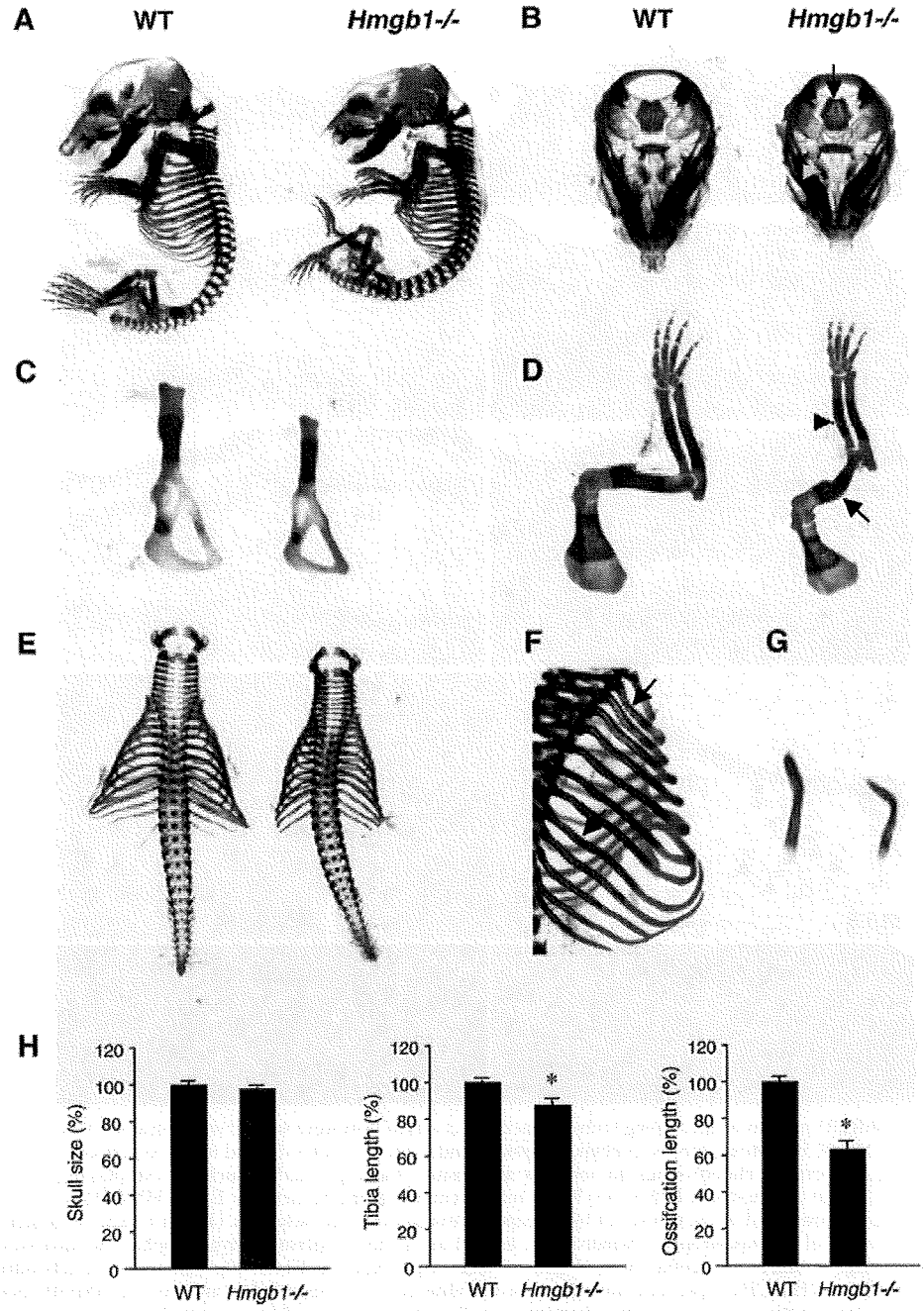

FIG. 1. Analysis of skeletal development in *Hmgb1*$^{-/-}$ mice by double staining with alcian blue and alizarin red. (A) *Hmgb1*$^{-/-}$ embryos (right) are smaller than wild-type (WT) littermates (left) at E16.5. (B) At this stage, facial and skull bones formed by intramembranous ossification appear similar between two groups, whereas sphenoid bones (arrowhead) and basioccipital (arrow) of the chondrocranium, which are formed by endochondral ossification, appear reduced in size and in intensity of alizarin red staining in *Hmgb1*$^{-/-}$ embryos. (C) The pelvis has smaller alizarin red-stained zones in *Hmgb1*$^{-/-}$ embryos. (D) The radius and ulna in *Hmgb1*$^{-/-}$ forelimbs are not only reduced in size and calcification, but bent (arrowhead); the humerus is often fractured (arrow). The thorax in *Hmgb1*$^{-/-}$ embryos shows severe hypoplasia accompanied by spinal scoliosis (E) and kyphosis (A). Ribs stained less intensely for alizarin red and are thin and bent (arrows) (F), and clavicles are hypoplastic and crooked in *Hmgb1*$^{-/-}$ embryos (G). (H) Statistical comparison between wild-type (n = 6) and *Hmgb1*$^{-/-}$ (n = 6) embryos at E16.5. The wild type is defined as 100%. Diameters of calvariae (skull size): wild-type, 100% ± 2.7%; mutant, 97.7% ± 2.2% (no statistical difference). Tibia length: wild-type, 100% ± 1.6%; mutant, 87.4% ± 6.9% ($P < 0.001$). Length of the ossified zone (alizarin red positive) of tibia: wild-type, 100% ± 6.9%; mutant, 63.6% ± 9.6% ($P < 0.0001$). The asterisk indicates a significant statistical difference ($P < 0.01$).

according to the method as described above. All experiments were performed at least twice in four replicates.

Three-dimensional pellet culture. Mice rib chondrocytes were prepared from the ventral parts rib cartilage of 2- to 4-day-old C57BL/6 mice as described previously (36). Human articular chondrocytes were isolated from human cartilage, and a primary cell culture was established (21). Both types of chondrocytes were cultured in three-dimensional cell pellets for 18 days as described before (5). Briefly, 1-ml aliquots containing 2 × 10^5 cells each were added to 15-ml

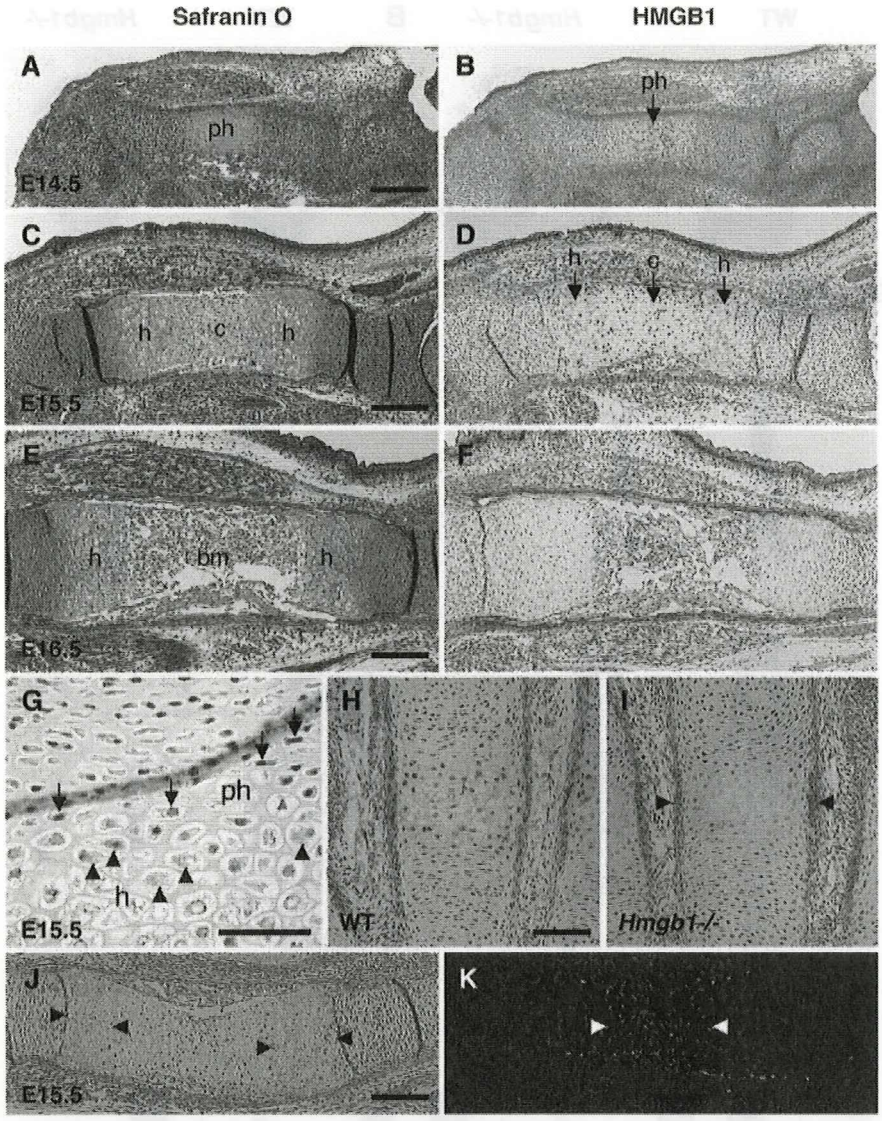

FIG. 2. Localization of HMGB1 protein in developing limbs. Adjacent sections of tibia were stained with safranin O (A, C, and E) and antibody to HMGB1 (B, D, and F). HMGB1 is expressed in the prehypertrophic chondrocytes at E14.5 (B) and in the hypertrophic chondrocytes at E15.5 (D). In contrast, resting and proliferating chondrocytes do not show any positive staining in either nuclei or cytoplasm. (F) Expression is robust in the limbs at E14.5 and E15.5 but attenuates at E16.5. (G) Large magnifications of the humerus at E15.5. HMGB1 is positive in the nuclei of prehypertrophic chondrocytes (arrows) and in the cytosol of hypertrophic chondrocytes (arrowheads). (H) At E16.5, metacarpal bones also show HMGB1 expression in the nuclei of prehypertrophic chondrocytes, as well as in the cytoplasm of hypertrophic chondrocytes. (I) The positive staining in hypertrophic cartilage is absent in sections from *Hmgb1*$^{-/-}$ metacarpal bones at E16.5. The staining in perichondrium is nonspecific (arrowheads). (J and K) Analysis of HMGB1 expression and apoptosis in radius at E15.5. Arrowheads indicate the HMGB1-positive cells (J) and TUNEL-positive cells presenting apoptosis of hypertrophic chondrocytes (K). ph, prehypertrophic cartilage; h, hypertrophic cartilage; c, calcified cartilage; bm, bone marrow. Scale bars: A to F, J, and K, 200 μm; G to I, 50 μm.

conical polypropylene centrifuge tubes (Becton Dickinson, San Diego, CA), and the cells were pelleted by centrifugation at 600 rpm for 5 min at room temperature. The cultures were maintained at 37°C in 5% CO_2 in a humidified incubator. Pellets were maintained up to 18 days in Dulbecco modified Eagle medium–F-12 supplemented with 50 μg of ascorbate phosphate (Sigma)/ml, 100 μg of pyruvate/ml, 1% penicillin-streptomycin (Gibco, Grand Island, NY), and 50 mg of ITS+Premix (Becton Dickinson, Bedford, MA; a final concentration of 6.25 μg of bovine insulin/ml, 6.25 μg of transferrin/ml, 6.25 ng of selenous acid/ml, 1.25 mg of bovine serum albumin/ml, and 5.35 μg of linoleic acid/ml)/ml. The medium was changed every 3 days. Cryostat-sectioned pellets were used for immunofluorescence assay. The supernatant of pelleted mouse rib chondrocytes and human articular chondrocytes was used for chemotaxis assay with or without addition of anti-HMGB1 IgY neutralizing HMGB1, a gift from Shino-Test (1), and control IgY (Promega, Madison, WI).

Quantitative PCR. Total RNA was extracted and oligo(dT)-primed cDNA was prepared from 500 ng of total RNA by using Superscript II (Invitrogen, Carlsbad, CA). The resulting cDNAs were analyzed by using the SYBR green system for quantitative analysis of specific transcripts according to the manufacturer's instructions (Applied Biosystems, Foster City, CA). All mRNA expression data were normalized to GAPDH expression in the corresponding sample. The primers used in real-time PCR are as follows: Col10a1, 5′-GCCTCAAATACCCTT TCTGC (sense) and 5′-GTGTCTTGGGGCTAGCAAGT (antisense); MMP13, 5′-GAAGACCTTGTGTTTGCAGAGC (sense) and 5′-CTCGGAGCCTGTCA ACTGTG (antisense); Hmgb1, 5′-GGCTGACAAGGCTCGTTATG (sense)

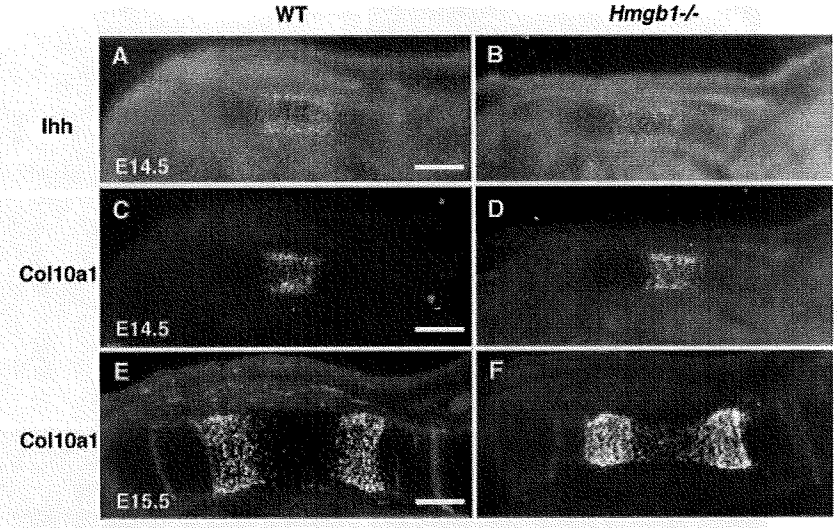

FIG. 3. Expression of chondrocyte differentiation markers in wild-type and *Hmgb1*$^{-/-}$ tibia. (A and B) Indian hedgehog (Ihh) is comparable between wild-type and *Hmgb1*$^{-/-}$ embryos at E14.5. (C to F) Col10a1 appears in the region of hypertrophic chondrocytes at E14.5 (C and D) and then declines in the most mature hypertrophic chondrocytes at the center of hypertrophic zones at E15.5 in both groups without an apparent difference between wild-type and mutant embryos (E and F). Scale bars, 200 μm.

and 5′-GGGCGGTACTCAGAACAGAA (antisense); and GAPDH, 5′-ATGT GTCCGTCGTGGATCTGA (sense) and 5′-GATGCCTGCTTCACCACCTT (antisense).

Statistics. The statistical analysis at present study was performed by using a two-tailed Student *t* test.

RESULTS

Analysis of skeletal development in *Hmgb1*$^{-/-}$ mice. We first examined bone and cartilage development in *Hmgb1*$^{-/-}$ mice. Since *Hmgb1*$^{-/-}$ mice die soon after birth (11), we analyzed *Hmgb1*$^{-/-}$ embryos. Alcian blue staining revealed no apparent difference in skeletal formation between *Hmgb1*$^{-/-}$ and wild-type littermate embryos at E13.5 (see Fig. S1A in the supplemental material). At E16.5, however, *Hmgb1*$^{-/-}$ embryos were smaller than wild-type embryos, suggesting a discrepancy during ossification (Fig. 1A). At this stage, facial and skull bones formed by intramembranous ossification appeared similar between the two groups, although the shape of *Hmgb1*$^{-/-}$ calvariae was relatively flat and depressed. In contrast, sphenoid bones and the basioccipital region of the chondrocranium, which are formed by endochondral ossification, appeared to be reduced in size and in intensity of alizarin red staining in *Hmgb1*$^{-/-}$ mice (Fig. 1B). Other bones formed by endochondral ossification, such as the pelvis, had smaller alizarin red-stained zones (Fig. 1C). The radius and ulna of *Hmgb1*$^{-/-}$ forelimbs were not only reduced in size and calcification but abnormally bent, suggesting a reduction of mineralization (Fig. 1D). Moreover, fractures were observed in the humeri of some (4 of 14) *Hmgb1*$^{-/-}$ mice. Thorax formation showed severe hypoplasia accompanied by spinal scoliosis (Fig. 1E) and kyphosis (Fig. 1A). Ribs stained less intensely for alizarin red and were thin and bent (Fig. 1F). The clavicles were hypoplastic and crooked (Fig. 1G). At E16.5, the diameters of calvariae were similar in both groups, whereas the lengths of the *Hmgb1*$^{-/-}$ tibias reached 87% of that of the wild type, and the alizarin-positive region reached 64% of the wild-type length (Fig. 1H). These findings suggest that in *Hmgb1*$^{-/-}$ mice endochondral ossification is impaired, whereas intramembranous ossification is only affected slightly and was not investigated further.

HMGB1 expression in normal growth plates. To investigate the mechanism of endochondral ossification defect in *Hmgb1*$^{-/-}$ embryos, we examined the localization of HMGB1 protein in the developing limbs of normal wild-type mice by immunohistochemistry. Safranin O staining showed that prehypertrophic cartilage appeared in the tibia at E14.5 (Fig. 2A), differentiating into hypertrophic cartilage, followed by calcified cartilage at E15.5 (Fig. 2C), and was replaced by bone marrow and bone trabeculae at E16.5 (Fig. 2E). By using the specific anti-HMGB1 polyclonal rabbit antibody which does not detect HMGB2 and HMGB3 (19), we found that HMGB1 was expressed in the prehypertrophic chondrocytes of the tibia at E14.5 (Fig. 2B) and in hypertrophic chondrocytes at E15.5 (Fig. 2D). Large magnifications of the humerus at E15.5 showed that HMGB1 was detected in the nuclei of prehypertrophic chondrocytes and in the cytosol of hypertrophic chondrocytes (Fig. 2G). On the other hand, resting and proliferating chondrocytes did not show any positive staining in either nuclei or cytoplasm. Not only large long bones but also other small long bones formed by endochondral ossification, such as metacarpal bones, exhibited HMGB1 expression in the nuclei of prehypertrophic chondrocytes, as well as in the cytoplasm of hypertrophic chondrocytes (Fig. 2H). This positive staining in hypertrophic cartilage was absent in *Hmgb1*$^{-/-}$ sections (Fig. 2I). These results indicate that HMGB1 is expressed and translocated from the nucleus to the cytosol during a specific stage of cartilage maturation. At the end of the cascade of chondrocyte maturation, terminal hypertrophic chondrocytes undergo apoptotic cell death (17). We analyzed HMGB1 expression and apoptosis in the radius at E15.5 and detected HMGB1 in hypertrophic chondrocytes (Fig. 2J) but not in terminal hypertrophic chondrocytes, which were positive for TUNEL staining

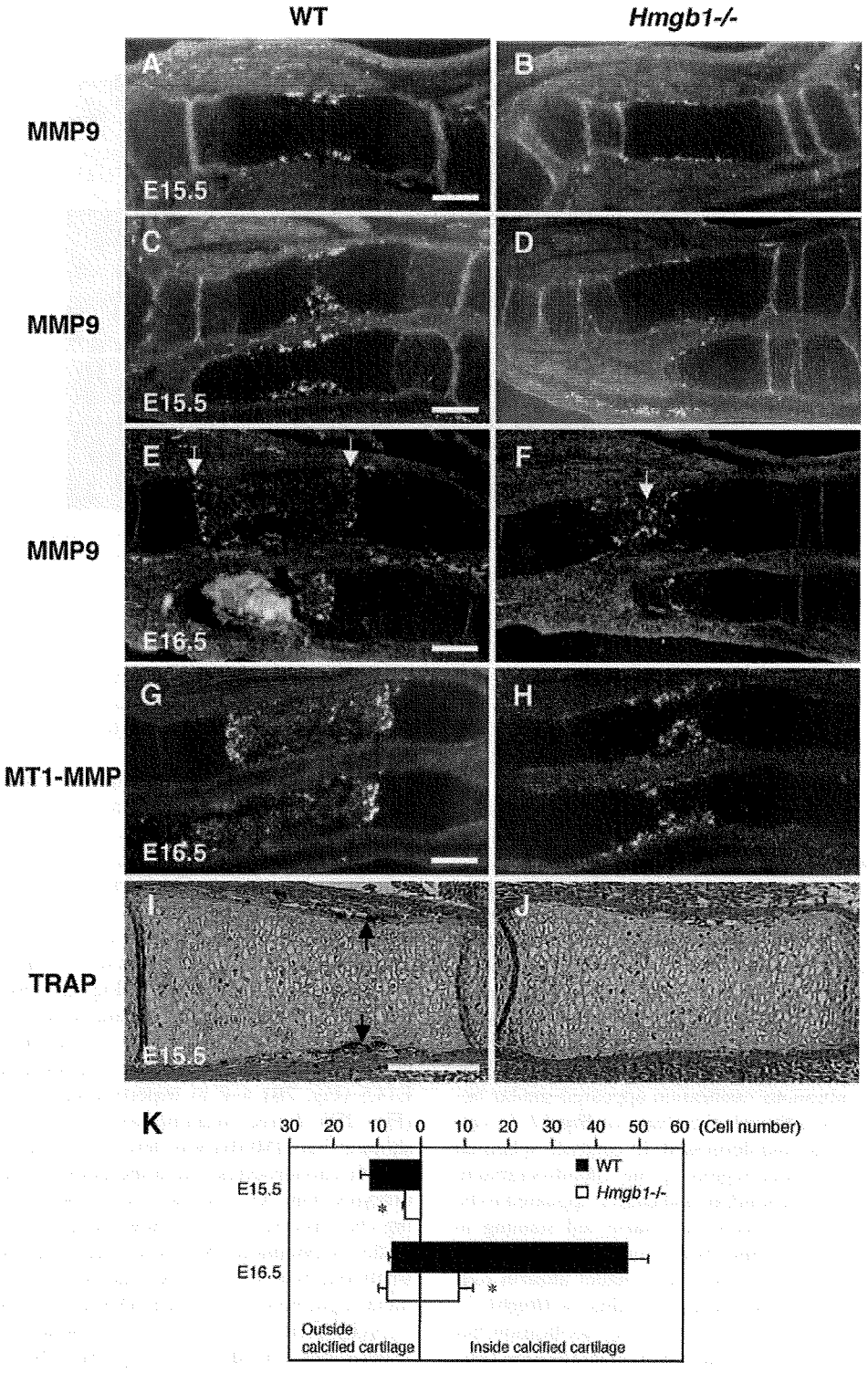

FIG. 4. Analysis of osteoclast markers in the primary ossification center. MMP9-positive osteoclastic cells are present in the perichondrium of the tibia (A) and radius and ulna (C) of wild-type embryos at E15.5 but are barely found in *Hmgb1*$^{-/-}$ bones (B and D). At E16.5, MMP9-positive cells are lining the transverse septae of cartilage-bone junctions that lead the vascular invasion front in wild-type radius (E, arrows), while they are still located in the primary ossification center in *Hmgb1*$^{-/-}$ bone (F, arrow). (G and H) The expression of MT1-MMP is similar to that of MMP9 in forelimbs at E16.5. TRAP staining indicates a significant reduction in the number of TRAP-positive cells in *Hmgb1*$^{-/-}$ tibia (J) compared to wild-type bone (I, arrows) at E15.5. (K) Quantification of the number of TRAP-positive cells in wild-type and *Hmgb1*$^{-/-}$ tibias. The total numbers of embryos were as follows: at E15.5, four wild-type and three mutant (pool of two littermates); and at E16.5, four wild-type and three mutant (pool of three littermates). The horizontal bars show the mean counts of TRAP-positive cells found either outside the calcified hypertrophic cartilage at the perichondrium-periosteum or inside the calcified hypertrophic cartilage. In both stages, there is a significant difference in the total number of TRAP-positive cells between wild-type and *Hmgb1*$^{-/-}$ mice (*, $P < 0.01$). Scale bars, 200 μm.

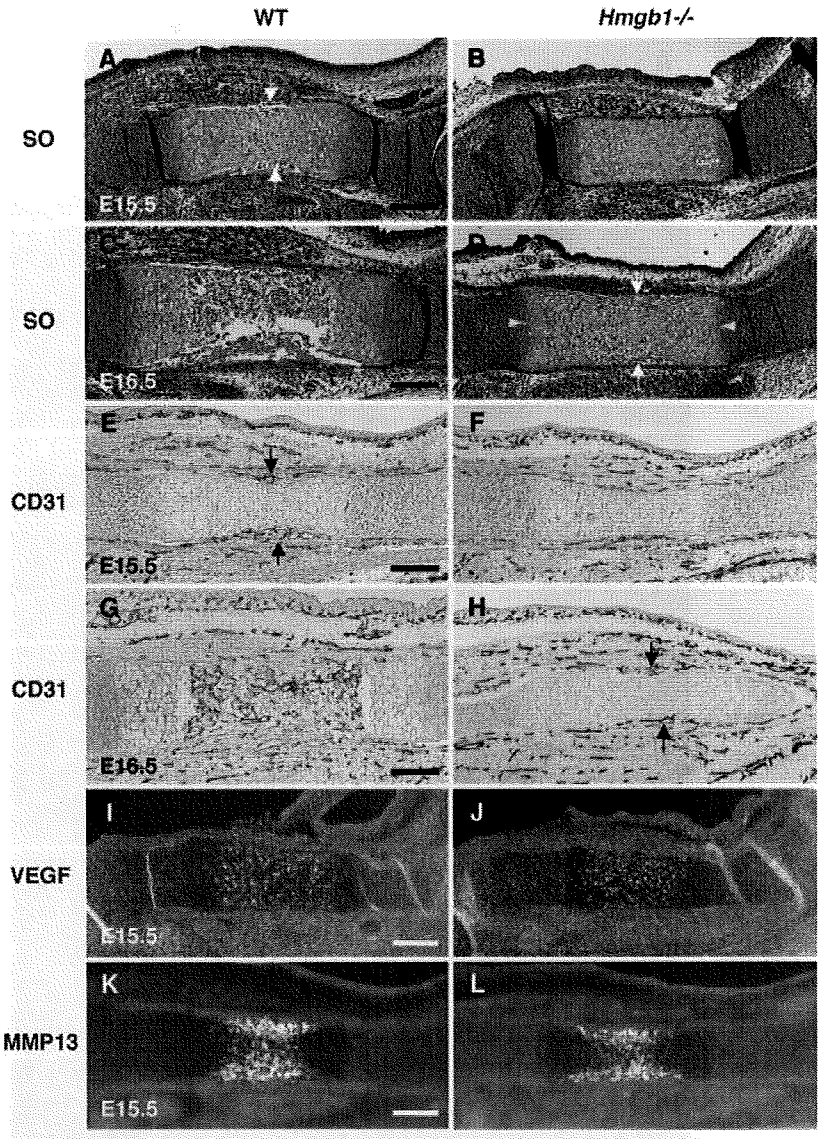

FIG. 5. Comparison of vascularization in wild-type and *Hmgb1*$^{-/-}$ skeletal elements during development. Safranin O staining (SO) of E15.5 tibias reveals that blood vessel invasion into the hypertrophic zone occurs in wild-type mice (A, arrows) but not in *Hmgb1*$^{-/-}$ mice (B). (C) At E16.5, hypertrophic cartilage is replaced by bone marrow and bone trabeculae in wild-type mice. (D) In contrast, the primary ossification center of *Hmgb1*$^{-/-}$ tibia is still intact with a wide hypertrophic zone (arrowheads) at the onset of blood vessel invasion (arrows). CD31 immunostaining shows that blood vessels start to invade the hypertrophic zone of wild-type tibia at E15.5 (E, arrows), but they are only surrounding the surface of *Hmgb1*$^{-/-}$ tibia (F). At E16.5, blood vessels have fully penetrated into the primary ossification center and distribute in bone marrow in wild-type tibia (G), whereas they still only surround the hypertrophic cartilage in *Hmgb1*$^{-/-}$ tibia (H, arrows). (I and J) VEGF expression in hypertrophic cartilage is similar for wild-type and *Hmgb1*$^{-/-}$ tibias at E15.5. (K and L) MMP13 expression in the calcified cartilage of wild-type tibia also resembles that of *Hmgb1*$^{-/-}$ tibias at E15.5. Scale bars, 200 μm.

(Fig. 2K), suggesting that HMGB1 was expressed just before cell death.

Impaired invasion of osteoclasts in *Hmgb1*$^{-/-}$ mice. Next, we sought to identify which process during endochondral ossification was disturbed by *Hmgb1* gene deficiency. To examine the rate of hypertrophic chondrocyte differentiation, we observed the expression of Indian hedgehog, a marker of prehypertrophic chondrocytes of cartilage elements (52), and found that it did not differ between wild-type (Fig. 3A) and *Hmgb1*$^{-/-}$ (Fig. 3B) tibias. Col10a1 appeared in the region of hypertrophic chondrocytes at E14.5 (Fig. 3C and D) and then declined in the most mature hypertrophic chondrocytes at the center of hypertrophic zones at E15.5 with a similar pattern in both groups (Fig. 3E and F). These findings indicate that *Hmgb1* gene deficiency does not affect the onset of cartilage maturation. In contrast, MMP9-positive osteoclastic cells (53) were distributed around the perichondrium in the tibias and radii of wild-type mice at E15.5 (Fig. 4A and C) but were barely detectable in *Hmgb1*$^{-/-}$ bones (Fig. 4B and D). At E16.5, the discrepancy became more remarkable. In the wild-

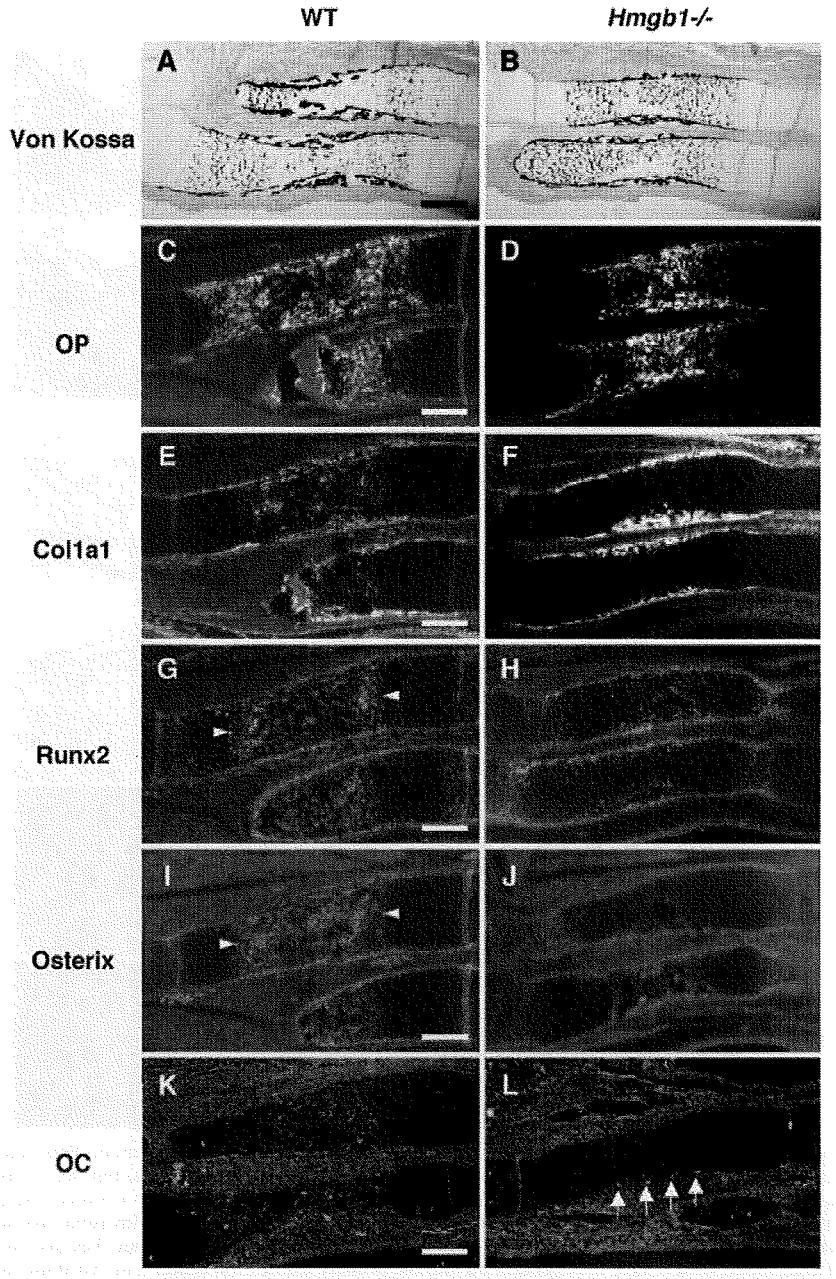

FIG. 6. Osteoblast differentiation markers in *Hmgb1*$^{-/-}$ forelimbs at E16.5. Von Kossa staining shows that calcified cartilage has not progressed to bone marrow in the radii and ulnas of *Hmgb1*$^{-/-}$ embryos (B) compared to wild-type embryos (A). Osteopontin (OP) is strongly expressed in the calcified hypertrophic cartilage of *Hmgb1*$^{-/-}$ bones (D), in which Col1a1-positive cells are not found (F). (C and E) In contrast, these osteoblastic cells are widely distributed in the bone marrow of wild-type bones. Runx2 and Osterix are highly expressed in the primary ossification center in wild-type radius (G and I, arrowheads), although they are barely detectable in *Hmgb1*$^{-/-}$ bones (H and J). Osteocalcin (OC) is found at the periphery of hypertrophic cartilage in *Hmgb1*$^{-/-}$ bones (L, arrows), while it appears in bone marrow in wild-type mice at E16.5 (K). Scale bars, 200 μm.

type radius, MMP9-positive cells were lining the transverse septae of cartilage-bone junctions that lead the vascular invasion front (Fig. 4E), whereas they were still located in the primary ossification center in *Hmgb1*$^{-/-}$ radius (Fig. 4F). The expression of MT1-MMP, which is highly expressed in osteoclasts (44), was similar to that of MMP9 (Fig. 4G and H). To confirm the apparent reduction in osteoclast numbers, we stained for TRAP and found significant reduction in the number of TRAP-positive cells in *Hmgb1*$^{-/-}$ tibias at E15.5 (Fig. 4I and J). Quantification of the number of these cells inside versus outside the calcified hypertrophic cartilage showed a significant difference between wild-type and *Hmgb1*$^{-/-}$ tibias (Fig. 4K). These findings demonstrate that osteoclast recruitment was suppressed in the *Hmgb1*$^{-/-}$ bones.

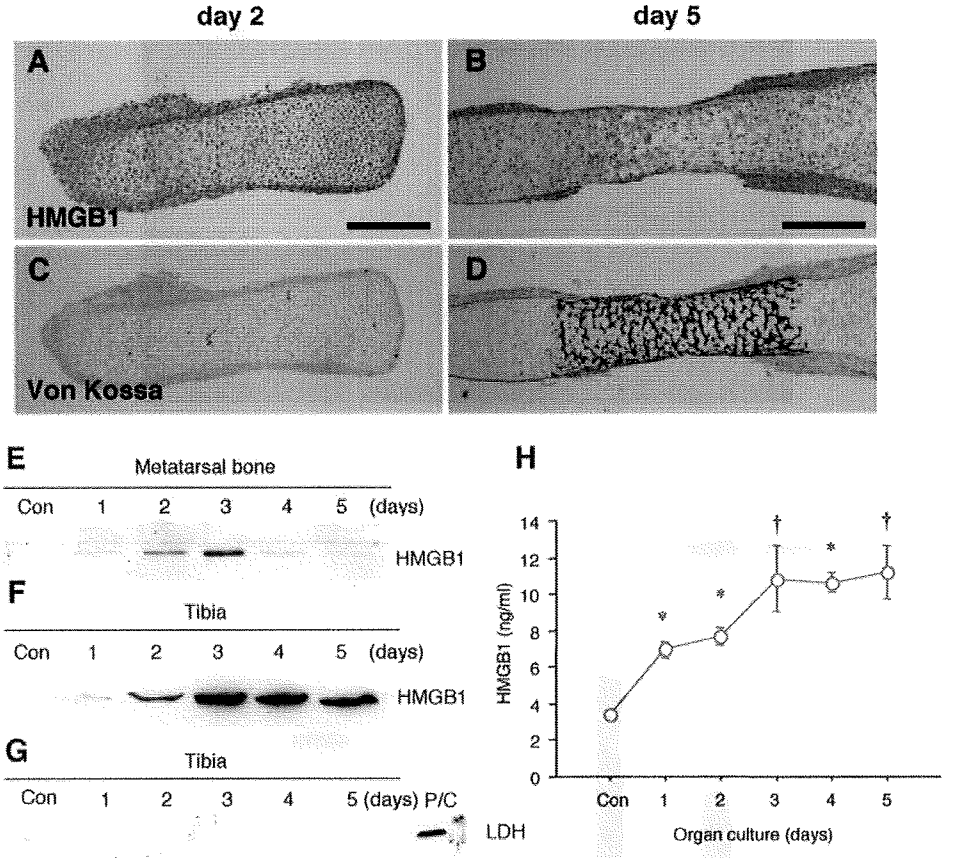

FIG. 7. HMGB1 is released extracellularly by developing cartilage. Metatarsal bones were isolated from wild-type embryos at E15.5 and cultured for up to 5 days. Immunohistochemistry reveals that HMGB1 is localized in hypertrophic chondrocytes of metatarsal bones on day 2 (A) and that expression is attenuated on day 5 (B). (C and D) Von Kossa staining with the adjacent sections shows that HMGB1 expression occurs in hypertrophic cartilage and not in calcified cartilage. Scale bars, 200 μm. Immunoblotting was carried out to determine the release of HMGB1 by cultured metatarsal bones. (E) HMGB1 is present in the supernatant with a peak 3 days after the start of organ culture, and then it decreases. (F) A large long bone, the tibia, which was isolated from embryos at E14.5, also releases HMGB1 in the supernatant. (G) The supernatant of the tibia does not contain LDH, a marker for cell necrosis; mouse rib chondrocytes undergoing necrosis are used as a positive control (P/C). (H) The HMGB1 level in the supernatant of tibia organ culture was quantified by ELISA. HMGB1 is released in a time-dependent fashion, which peaked on days 3, 4, and 5 at concentrations of 10.8 ± 5.4, 10.7 ± 1.6, and 11.2 ± 4.4 ng/ml, respectively. Statistically significant differences from the HMGB1 level in control supernatant are indicated (*, $P < 0.01$; †, $P < 0.05$).

Altered vascularization of skeletal elements in *Hmgb1*$^{-/-}$ mice during development. MMP9-positive cells enter the mesenchyme surrounding the bone rudiments and migrate together with endothelial cells through the nascent bone collar at the primary ossification center (15). Thus, we examined the vascularization in skeletal elements of *Hmgb1*$^{-/-}$ mice. Safranin O staining revealed that blood vessel invasion into the hypertrophic zone occurred in wild-type tibias at E15.5 (Fig. 5A) but not in *Hmgb1*$^{-/-}$ tibias (Fig. 5B). At E16.5, hypertrophic cartilage was replaced by bone marrow and bone trabeculae in wild-type mice (Fig. 5C). In contrast, the primary ossification center of *Hmgb1*$^{-/-}$ tibias was still intact with a wide hypertrophic zone and only the onset of blood vessel invasion (Fig. 5D). Using CD31 (PECAM) antibody, which is a marker of endothelial cells, we performed immunostaining and found that blood vessels started to invade the hypertrophic zone of wild-type tibia at E15.5 (Fig. 5E), but they were only on the surface of *Hmgb1*$^{-/-}$ tibia (Fig. 5F). At E16.5, blood vessels had fully penetrated into the primary ossification center and distributed in bone marrow in wild-type tibia (Fig. 5G), whereas they were still only surrounding the hypertrophic cartilage in *Hmgb1*$^{-/-}$ bone (Fig. 5H). At the growth plate, hypertrophic cartilage expresses VEGF, and inhibition of VEGF activity blocks the recruitment of MMP9-positive and TRAP-positive cells, as well as endothelial cells (17). We found no difference in VEGF expression in hypertrophic cartilage between wild-type and *Hmgb1*$^{-/-}$ tibia at E15.5 (Fig. 5I and J). MMP13, which is expressed by both terminal hypertrophic chondrocytes and osteoblasts, is also important for the vascularization of hypertrophic cartilage because it degrades native collagen, a major component of the hypertrophic cartilage (47). MMP13 expression in the calcified cartilage of the wild-type tibia resembled that of the *Hmgb1*$^{-/-}$ tibia (Fig. 5K and L). Taken together, these findings suggest that the cell invasion into hypertrophic cartilage by endothelial cells was disrupted in *Hmgb1*$^{-/-}$ bones during the process of endochondral ossification, although VEGF and MMP13 expression was unaltered.

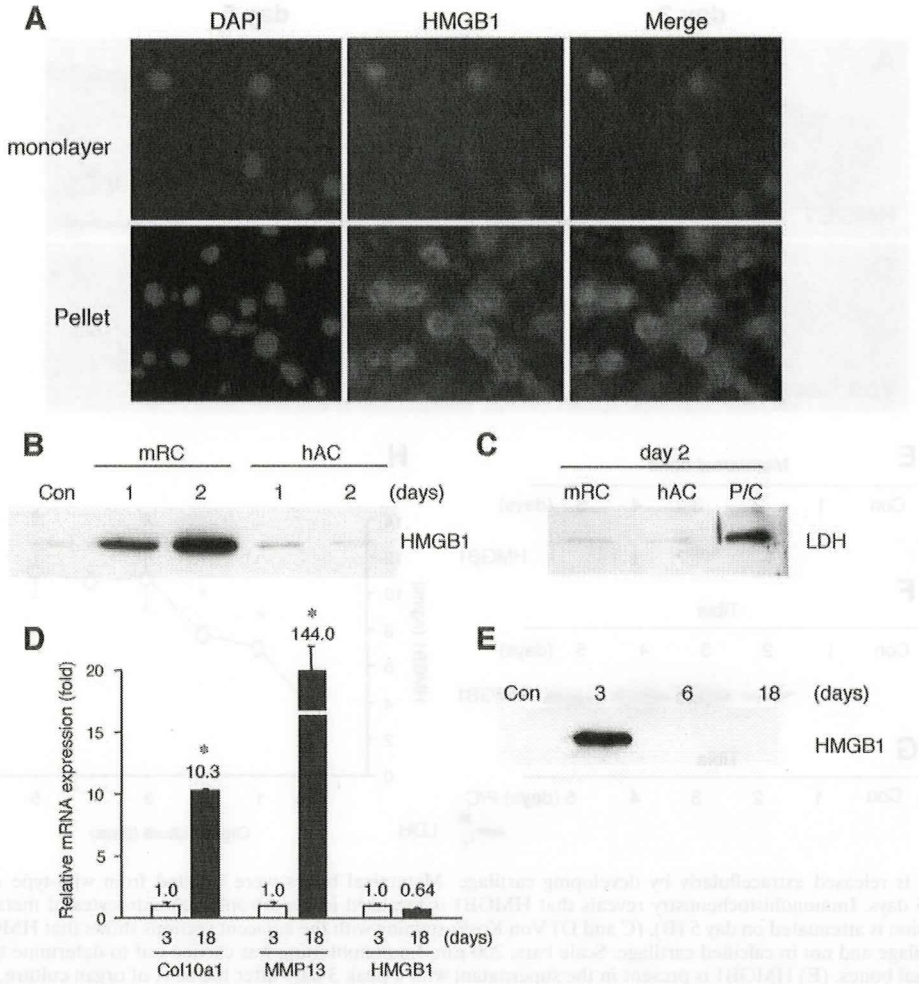

FIG. 8. HMGB1 release from differentiating cultured rib chondrocytes. (A) Immunofluorescence assay shows that monolayer rib chondrocytes isolated from the ventral parts of mice rib cartilage express HMGB1 only in the nucleus, whereas in pelleted rib chondrocytes cultured for 2 days HMGB1 is localized in the cytosol. The extracellular release of HMGB1 was verified with immunoblotting. (B) HMGB1 was determined in the supernatant of pelleted mice rib chondrocytes (mRC) on days 1 and 2, whereas human articular chondrocytes (hAC) do not release HMGB1 in pellet culture. (C) Immunoblotting with LDH antibody shows that this secretion is independent of necrotic cell death. The positive control (P/C) is the same sample as shown in Fig. 7G. (D) During the culture of pelleted mRC for 18 days, quantitative PCR demonstrates that the mRNA level of cartilage maturation markers such as Col10a1 and MMP13 increases significantly on day 18, although that of HMGB1 is unchanged. (E) Only the supernatant on day 3 contains HMGB1. Statistically significant differences from mRNA expression on day 3 are indicated, respectively (*, $P < 0.01$).

Osteogenesis in *Hmgb1*$^{-/-}$ mice. As shown in Fig. 1, *Hmgb1*$^{-/-}$ forelimbs appeared to be reduced in size and calcification and were abnormally bent or fractured. Since these findings suggest a reduction of bone mineralization, we investigated osteoblast differentiation in *Hmgb1*$^{-/-}$ bones. Using von Kossa staining, we found that calcified cartilage had progressed to bone marrow in the radii and ulnas of wild-type mice (Fig. 6A) but not in *Hmgb1*$^{-/-}$ mice (Fig. 6B). Osteopontin, a hypertrophic cartilage marker as well as an osteoblast marker (35), was strongly expressed in the calcified hypertrophic cartilage of *Hmgb1*$^{-/-}$ bones (Fig. 6D) in which Col1a1-positive cells, an early marker of osteoblast differentiation (18), were not found; these cells were accumulated at the collar surrounding the growth plate (Fig. 6F). In contrast, Col1a1-positive cells were widely distributed in the bone marrow of wild-type mice (Fig. 6E), suggesting that osteoblast invasion was suppressed in *Hmgb1*$^{-/-}$ limbs. The essential transcription factors for osteoblast differentiation, Runx2 (27) and Osterix (34), were highly expressed in the primary ossification center of the wild-type radius (Fig. 6G and I), whereas they were barely detectable in the *Hmgb1*$^{-/-}$ bones (Fig. 6H and J). Osteocalcin, which is thought to be a terminal marker for osteoblastic maturation (29), was found at the periphery of hypertrophic cartilage in *Hmgb1*$^{-/-}$ bones at E16.5 (Fig. 6L); however, it appeared in the bone marrow at E17.5 (data not shown) rather than at E16.5 as in wild-type mice (Fig. 6K). Thus, the delay in primary ossification of *Hmgb1*$^{-/-}$ hypertrophic cartilage was coupled to a delay in recruitment of osteoblasts, suggesting that subsequent osteoblastic differentiation progressed similarly in wild-type and *Hmgb1*$^{-/-}$ mice.

HMGB1 is released from differentiating cartilage in organ culture. To examine the secretion of HMGB1 from chon-

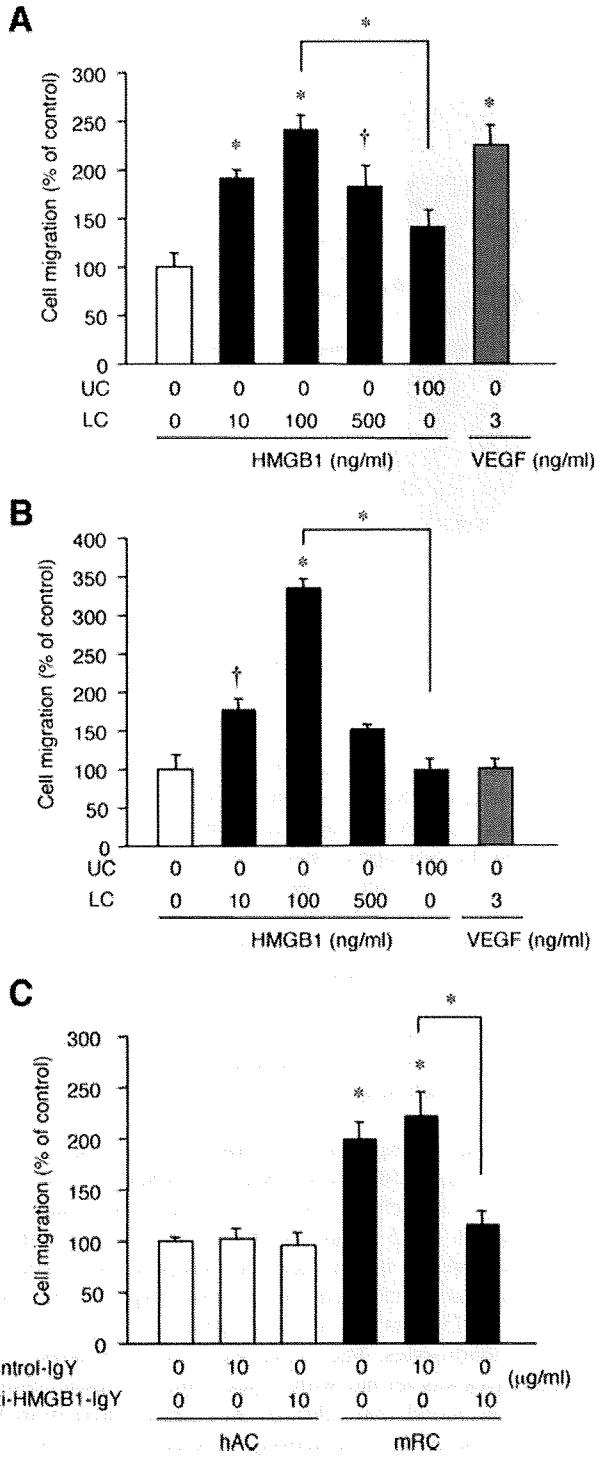

FIG. 9. Chondrocyte-secreted HMGB1 is a chemoattractant for osteoclasts. The chemotactic effect of recombinant HMGB1 on osteoclasts was examined by Boyden chambers with or without addition of HMGB1 to either the lower chamber (LC) or the upper chamber (UC) as indicated. (A) HMGB1 recruits osteoclasts at 10 ng/ml, and efficacy peaks at 100 ng/ml. The addition of HMGB1 to the upper chamber does not significantly activate osteoclast invasion. (B) HMGB1 also recruits osteoblastic MC3T3-E1 cells with a tendency similar to that described above, although VEGF does not. Statistically significant differences from control migrations without added chemoattractants are indicated, respectively (*, $P < 0.01$; †, $P < 0.05$). (C) Chemotaxis assay using the supernatant of pelleted mice rib chondrocytes (mRC) and human articular chondrocytes (hAC) after 3 days culture. The supernatant of hAC does not recruit osteoclasts, whereas that of mRC attracts osteoclasts significantly, and this effect is abrogated by addition of anti-HMGB1 IgY. Cell migration is shown as mean ± the standard deviation of four replicates. Statistically significant differences from control migrations by the supernatant of hAC are indicated (*, $P < 0.01$).

drocytes, we used the cartilage organ culture system (20). Metatarsal bones were isolated from embryos at E15.5 and cultured in conditioned medium for up to 5 days. Immunohistochemistry revealed that HMGB1 was localized in hypertrophic chondrocytes on day 2 (Fig. 7A) and that expression was attenuated on day 5 (Fig. 7B). Von Kossa staining of the adjacent sections indicated that this expression occurred in hypertrophic cartilage and not in calcified cartilage (Fig. 7C and D). Using immunoblotting, we determined that HMGB1 was present in the supernatant, with a peak 3 days after the start of organ culture, and then it decreased (Fig. 7E), showing that HMGB1 was released into the medium by hypertrophic chondrocytes. This result was reproduced with a large long bone, the tibia, which was isolated from the embryos at E14.5 (Fig. 7F). Immunoblotting with LDH antibody was negative, indicating that HMGB1 was actively secreted and not released passively as a consequence of necrotic cell death (Fig. 7G). Using ELISA, we quantified the HMGB1 protein released into the medium of tibia organ culture and found that it peaked on days 3 through 5 at concentrations of >10 ng/ml (Fig. 7H).

HMGB1 is released specifically from hypertrophic chondrocytes. It has been previously demonstrated that HMGB1 is released from osteoclasts and osteoblast-like cells (12, 42). To prove that the release of HMGB1 into the supernatant was from chondrocytes in organ culture, we used pellet cultures of rib growth plate chondrocytes, since this culture system mimics in vivo cartilage differentiation (5). Monolayer chondrocytes isolated from the ventral parts of mouse rib cartilage expressed HMGB1 only in the nucleus; however, when cultured as differentiating cell pellets, HMGB1 was localized in the cytosol (Fig. 8A). Extracellular HMGB1 was detected in the supernatant of pelleted rib chondrocytes on days 1 and 2; in contrast, articular chondrocytes, which do not differentiate to hypertrophic cartilage under the three-dimensional condition such as pellet or alginate culture (6, 40), did not release HMGB1 (Fig. 8B). Immunoblotting with LDH antibody showed that HMGB1 release was not caused by necrotic cell death (Fig. 8C). In addition, to examine HMGB1 expression in longer-term cultures, we maintained the rib chondrocyte pellets for 18 days. Quantitative PCR demonstrated that mRNA of cartilage maturation markers such as Col10a1 and MMP13 increased significantly, showing that chondrocyte differentiation had occurred (Fig. 8D). Only the medium from day 3 contained HMGB1 (Fig. 8E), although the mRNA level of HMGB1 did not significantly change between day 3 and 18. These results indicate that HMGB1 is secreted during the early phase of cartilage maturation.

HMGB1 is a chemoattractant for osteoclasts and osteoblasts. As we showed in Fig. 4, 5, and 6, *Hmgb1*$^{-/-}$ embryos

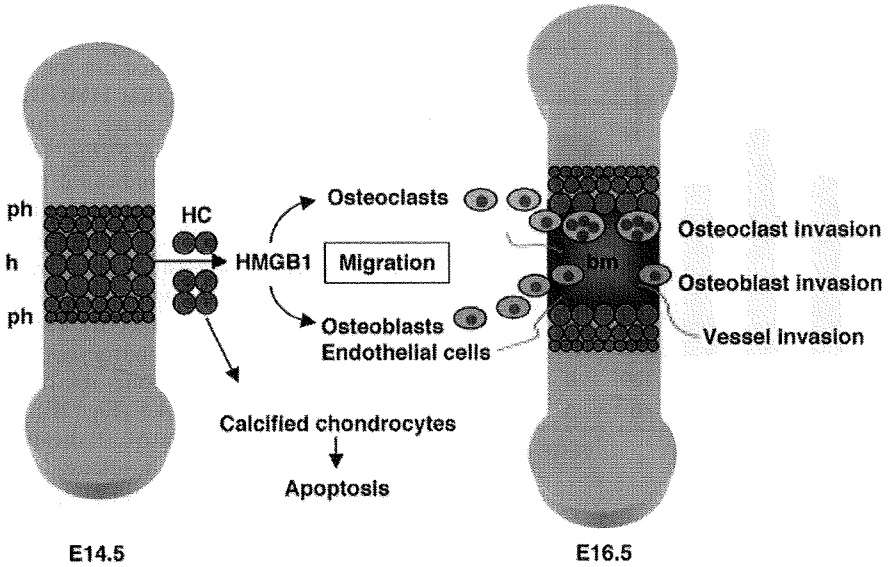

FIG. 10. Role of HMGB1 in skeletal development. During endochondral ossification, a region of resting chondrocytes transforms into a zone of proliferating chondrocytes that then undergo hypertrophy and subsequently apoptosis. HMGB1 is released from the hypertrophic chondrocytes just before undergoing programmed cell death; it acts as an extracellular signal for the migration of osteoclasts, osteoblasts, and endothelial cells that replace cartilage with bone and bone marrow. ph, prehypertrophic cartilage; h, hypertophic cartilage; bm, bone marrow; HC, hypertrophic chondrocytes.

were defective in invasion by TRAP- and Col1a1-positive cells, as well as CD31-positive cells, at the primary ossification center. Since HMGB1 has chemotactic effects on endothelial cells (32, 46), we tested for similar effects on osteoclasts and osteoblasts. Recombinant HMGB1 at 10 ng/ml recruited osteoclasts in Boyden chambers, and peak migration occurred at 100 ng/ml; this level of efficacy was similar to that of VEGF used as a positive control (22) (Fig. 9A). Addition of HMGB1 to the upper chamber did not significantly activate osteoclast migration. HMGB1 also induced chemotaxis for MC3T3-E1 osteoblast-like cells with a tendency similar to that described above (Fig. 9B), although VEGF did not (16). These findings suggest that osteoclast and osteoblast invasion at the primary ossification center might be a direct effect of HMGB1-induced chemoattraction.

Finally, we investigated whether HMGB1 released by differentiating chondrocytes could promote osteoclast migration. Using the supernatant of pelleted rib chondrocytes and articular chondrocytes cultured for 3 days (see Fig. S2 in the supplemental material), we compared the chemotactic effect for osteoclasts. The supernatant of articular chondrocytes did not recruit osteoclasts; however, the supernatant of rib chondrocytes attracted osteoclasts significantly, and the effect was abrogated by neutralizing anti-HMGB1 IgY (Fig. 9C). This result supports our hypothesis that differentiating chondrocytes could regulate cell migration directly via HMGB1 secretion.

DISCUSSION

This study demonstrates that the stage-specific secretion of HMGB1 in cartilage regulates endochondral ossification, at least in part, by acting as a chemotactic factor for osteoclasts and osteoblasts, as well as endothelial cells. We examined skeletal development in *Hmgb1*$^{-/-}$ embryos and found significant alterations in the bones formed by endochondral ossification, whereas calvariae, which are formed by intramembranous ossification, were somewhat misshapen, but the effect was slight, and the cartilage formation was not affected. The analysis of *Hmgb1*$^{-/-}$ limb sections revealed that the onset of cartilage differentiation was similar in *Hmgb1*$^{-/-}$ and wild-type embryos; however, the invasion of TRAP- and Col1a1-positive cells, as well as CD31-positive cells, into the primary ossification center was remarkably impaired in *Hmgb1*$^{-/-}$ limbs. Thus, the *Hmgb1*$^{-/-}$ growth plates are strikingly lengthened and deficient in osteoblast and osteoclast invasion as well as vascularization, which may result in weak bones that can bend or fracture.

To examine the expression of HMGB1 in developing limbs, we used in situ hybridization: HMGB1 mRNA expression was ubiquitous in the cells of all zones of the growth plate from E14.5 through E16.5 (data not shown). In contrast, HMGB1 protein was present in the nuclei of prehypertrophic chondrocytes in tibia at E14.5 and in the cytosol of hypertrophic chondrocytes at E15.5 but was not detectable in resting and proliferating chondrocytes. The active secretion of HMGB1 from chondrocytes was verified with organ culture and pellet culture systems; we found that HMGB1 was translocated from the nucleus to the cytosol and actively secreted at the early phase of chondrocyte differentiation, but the secretion ceased at the late phase. Interestingly, secretion from pelleted rib chondrocytes occurred actively without added any stimulatory factor, whereas articular chondrocytes did not release HMGB1 in pellet culture. Chondrocyte-secreted HMGB1 was sufficient to chemoattract osteoclasts and osteoblasts, as well as endothelial cells as previously shown by others (32, 46). These findings suggest that HMGB1 released from hypertrophic chondrocytes may regulate skeletal development by controlling cell invasion